

**Interaction between TRPV3 and TMEM79 in mouse
keratinocytes and its physiological significance**

Lei, Jing

Doctor of Philosophy

The Graduate University for Advanced Studies, SOKENDAI

School of Life Science

Department of Physiological Sciences

2022

Table of Contents

Abstract	- 3 -
Introduction	- 6 -
TRPV3 sensitization and modulation	- 6 -
TRPV3 as a thermosensor	- 8 -
TRPV3 in cutaneous physiology and pathophysiology.....	- 9 -
TMEM79: an emerging cutaneous target	- 10 -
Materials and Methods	- 13 -
Animals and genotyping.....	- 13 -
Cell culture	- 13 -
DNA construction.....	- 14 -
Primary mouse keratinocyte isolation and culture	- 14 -
Transient transfection	- 15 -
Whole-cell voltage-clamp	- 15 -
Ca ²⁺ imaging.....	- 16 -
Co-immunoprecipitation.....	- 16 -
Biotinylation of cell surface proteins	- 17 -
Western blot.....	- 18 -
Immunofluorescence	- 18 -
Duolink proximity ligation assay	- 19 -
RT-PCR	- 20 -
Scratching behavior in mice	- 20 -
Thermal behavioral assay	- 20 -
Results	- 22 -
TMEM79 reduces TRPV3-mediated currents, but not TRPV4	- 22 -
TMEM79 downregulates TRPV3 protein levels	- 23 -
TRPV3 and TMEM79 form a complex	- 23 -
TMEM79 alters TRPV3 localization.....	- 24 -
TMEM79 restricts TRPV3 mainly in the ER and causes TRPV3 degradation in the lysosome	- 25 -
Potential interaction between TRPV4 and TMEM79	- 26 -
Keratinocytes exhibit three distinct responses to 2-APB and GSK101	- 26 -

TMEM79 regulates TRPV3-mediated currents and calcium influx in primary skin keratinocytes.....	- 27 -
TMEM79-deficient mice exhibit less scratching induced by carvacrol.....	- 28 -
TMEM79-deficient mice have a pronounced alteration in temperature sensing	- 29 -
<i>Discussion</i>	- 31 -
<i>References</i>	- 38 -
<i>Figures</i>	- 48 -
<i>Tables</i>	- 78 -
<i>Acknowledgments</i>	- 84 -

Abstract

TRPV3, a warmth-activated ($> 33^{\circ}\text{C}$) cation-permeable transient receptor potential (TRP) ion channel, is predominantly expressed in skin keratinocytes and participates in various physiological processes ranging from somatosensation to inflammation. Although some progress has been made in understanding TRPV3, numerous issues remain to be addressed. First, modulation of ion channels could affect their subcellular localization, channel properties, or gating, which is considered important for physiological changes in organisms. Despite TRPV3 being activated by a wide range of external stimuli and its channel activities being regulated by several intracellular factors, little is known about TRPV3-associated proteins. Furthermore, although TRPV3 knockout mice exhibit a defective preference to warm temperature, it remains controversial whether TRPV3 directly contributes to thermosensation. Moreover, expression levels of TRPV3 are increased in isolated keratinocytes from patients with atopic dermatitis (AD), a common chronic skin disease associated with inflammation, itch, and skin barrier dysfunction. Multiple TRPV3 gain-of-function mutations are also associated with a hereditary skin disease, olmsted syndrome (OS), characterized by abnormal keratinization and severe itch. However, the underlying mechanism by which TRPV3 is involved in such cutaneous diseases is still poorly understood. Interestingly, transmembrane protein 79 (TMEM79), a putative five-pass transmembrane protein, is similarly highly expressed in skin keratinocytes. TMEM79 is associated with skin barrier formation and pathogenesis in AD-like mice. Therefore, I proposed the straightforward hypothesis that both TRPV3 and TMEM79 are likely to function together in the skin.

In this study, I first evaluated whether TMEM79 could modulate TRPV3-mediated currents by performing whole-cell patch-clamp experiments and found that mouse TMEM79 was capable of suppressing 2-aminoethoxy diphenyl borate (2-APB)-induced current amplitudes in HEK293 cells transiently expressing mouse TRPV3. In line with this, further biotinylation assays and co-immunoprecipitation revealed that TMEM79 could decrease the expression levels of plasma membrane TRPV3 through a physical interaction. In addition, with co-expression of TMEM79, immunofluorescence staining with different organelle markers showed that TRPV3 was largely retained in the endoplasmic reticulum (ER). Meanwhile, some TRPV3 was localized within lysosomes, suggesting that TMEM79 promoted TRPV3 degradation through the lysosomal pathway, which is consistent with a reduction in TRPV3 total protein levels as determined by Western blot. Taken together, these findings indicate that TMEM79 inhibits the membrane trafficking of TRPV3 while simultaneously facilitating the degradation of TRPV3, thereby affecting TRPV3-related activities.

Consistent with the results in HEK293 cells, 2-APB-induced TRPV3 currents were larger in primary mouse keratinocytes lacking TMEM79. This was supported by subsequent Ca^{2+} imaging in which the application of either a cocktail 2-APB/carvacrol or heat resulted in larger Ca^{2+} influxes in keratinocytes from TMEM79^{-/-} mice than from wild-type mice. Taken together, these findings demonstrate that TMEM79 is required for the regulation of TRPV3 channels in mouse primary keratinocytes, implying a potential physiological interaction *in vivo*.

To understand the significance of the interaction between TRPV3 and TMEM79 *in vivo*,

I first sought to confirm that TRPV3 played a role in warmth sensing by conducting a behavioral assay using a thermal gradient ring. Surprisingly, I found that TMEM79^{-/-} mice displayed a strong preference for warmer temperatures compared to wild-type and TRPV3^{-/-} mice. This is likely caused by higher endogenous TRPV3 protein levels in keratinocytes when TMEM79 is deleted. These findings suggest that TMEM79 may be involved in temperature sensation through the modulation of TRPV3 channel density in the plasma membrane of skin keratinocytes.

Together, this project reveals a novel interaction between TRPV3 and TMEM79, in which TMEM79 functions as a modulator of TRPV3 by affecting TRPV3 trafficking. Dysfunction of TRPV3 primarily contributes to skin physiology and pathophysiology. Therefore, this interaction provides additional insight into our overall understanding of skin pathogenesis. As a future vision, the modulation of cell surface TRPV3 may represent a valuable therapeutic approach for the treatment of skin diseases. Of particular therapeutic importance, channel activity can be modulated by the number of ion channels present. Based on studies by myself and others, TMEM79 is likely to function as an enzyme, and it is possible that we can indirectly manage TRPV3 activity for the treatment of skin conditions by regulating TMEM79.

Given that TRPV3 is activated by human body temperature, it is proposed to be a thermosensor in our skin by conveying temperature information from keratinocytes to the brain. However, the mechanism by which an organism orchestrates thermotransduction in the skin needs further investigation. Modulation of TRPV3 by its associated proteins such as TMEM79 could be one intriguing approach for further elucidating these mechanisms.

Introduction

Transient receptor potential (TRP) channels are non-selective cation ion channels. They were initially termed “transient receptor potential” because of the abnormal transient receptor potential found in phototransduction of the eyes of mutant *Drosophila melanogaster*^{1,2}. Later, TRP channels were found to be widely distributed in various tissues across vertebrates and invertebrates. In humans, 27 TRP channels have been identified and are divided into six subfamilies based on their amino acid sequences: TRPA (ankyrin, TRPA1), TRPC (canonical, TRPC1, 3-7), TRPV (vanilloid, TRPV1-6), TRPM (melastatin, TRPM1-8), TRPML (mucolipin, TRPML1-3), and TRPP (polycystin, TRPP1-3). All TRP channels consist of six transmembrane domains (S1-6) with intracellular N- and C- termini, and function as a tetramer complex^{3,4}. TRPV3 is a member of the TRPV family and shares the closest similarities with human TRPV1 (43%), TRPV4 (42%), and TRPV2 (41%) sequences at the amino acid level⁵. TRPV3 is predominately expressed in skin keratinocytes but hardly detected in the brain, spinal cord, or dorsal root ganglia (DRG) in rodents⁶. TRPV3 is also functionally present in the nasal, oral, corneal, lung, and distal colon epithelia⁷⁻¹⁰. Similar to other TRP channels, TRPV3 is involved in many physiological and pathophysiological processes¹¹.

TRPV3 sensitization and modulation

TRPV3 can be activated by heat (> 33°C) and some monoterpenes which are derived from natural plants, such as camphor, menthol, carvacrol, or thymol, as well as synthetic chemicals, like 2-APB^{8,12,13}. Some amino acid residues underlying TRPV3 activation have been studied by mutagenesis or cryo-EM. For instance, 2-APB-induced currents were abolished by multiple cytoplasmic mutations such as H426 and R696^{14,15}. Although the specific antagonists of TRPV3 have been limited in number, a few recent

studies have identified several selective and potent chemicals (citrusinine-II, osthole, and dyclonine) although they do not share the same inhibitory mechanisms¹⁶⁻¹⁹. TRPV3 sensitization in standard medium shows a pronounced outward rectification and is unique in its progressive response to repeated stimulations, which is different from desensitization in other TRP channels^{6,18,20,21}. Calcium ions have been implicated to play a role in modulation of the above channel process, in which intracellular Ca^{2+} coupled with calmodulin (CaM) causes TRPV3 sensitization^{20,22}. This regulation is further evidenced by direct binding between CaM and the TRPV3-ankyrin-repeat domain (ARD)^{22,23}. Extracellular Ca^{2+} is also able to slow down TRPV3 activation by direct action within the pore loop²². Moreover, TRPV3 activation is potentiated intracellularly by protons^{24,25}, some unsaturated fatty acids, such as arachidonic acid²⁶, and inhibited by phosphatidylinositol (4,5) biphosphate ($\text{PI}(4,5)\text{P}_2$)²⁷, ATP²³, and magnesium ions²⁸.

Most TRP channels, including TRPV3, conduct their functions predominantly at the plasma membrane. Therefore, the modulation of intracellular translocation or membrane trafficking of TRP channels is associated with their physiological state, which theoretically allows for therapeutic development through targeting cell surface modulation of these ion channels²⁹. Accordingly, many TRP-binding proteins have been applied in experiments aimed at modulating protein trafficking in thermo-TRPV1-4, TRPM3, TRPM8, and TRPA1 channels²⁹. Among this research, studies pertaining to TRPV3 have been limited but profound. For instance, sorting nexin 11 (SNX11), a cellular trafficking protein, was shown to promote TRPV3 degradation in lysosomes and inhibit membrane trafficking³⁰.

TRPV3 as a thermosensor

Thermosensation is a crucial sensory process for survival of all organisms. In mammals, many thermoreceptors that respond to temperature stimuli have been identified. Over the past two decades, TRP ion channels have attracted a surge of attention from researchers after TRPV1 was cloned as a nociceptor in sensory neurons^{31,32}. To date, 11 thermo-sensitive TRP family members have been identified, but only a few of them are thought to be required for sensing temperature *in vivo*. TRPV1 knockout mice exhibit a longer latency in responding to noxious heat, suggesting TRPV1 is needed for noxious temperature sensation³³. Furthermore, the withdrawal response to noxious heat is abolished in TRPV1-TRPM3-TRPA1 triple knockout mice, revealing the potential roles of TRPM3 and TRPA1 in noxious heat sensing in addition to TRPV1³⁴. TRPM8 as a cold-sensor is directly involved in detecting cold *in vivo*³⁵. Different from the above thermo-TRP channels with high expression in DRGs, TRPV3 and TRPV4 are suggested to be important for warmth sensation because of their activation in keratinocytes by innocuous temperature, but TRPV3- or TRPV4-deficient mice preferred cooler or warmer floor temperatures, respectively^{21,36}. However, the direct contribution of keratinocytes or the indirect contact between keratinocytes and nerve endings embedded in the skin has not been well elucidated. On one hand, high levels of TRPV3 expression in skin keratinocytes suggest that TRPV3 is likely to modulate thermotransduction through intermediators released from keratinocytes such as ATP and nitric oxide^{37,38}. On the other hand, it was recently proposed that keratinocytes are directly required for conveying temperature information *in vivo*, implying a potential contribution of TRPV3 to warmth sensation *in vivo*³⁹. It is likewise possible that TRPV3 channel activity influences other physiological changes that are crucial for thermosensation. Nevertheless, one study proposed that TRPV3 exerts only a mild

influence on temperature preference, but this was likely attributed to different genetic backgrounds⁴⁰. These above debates are a reflection of the functional complexity of TRPV3 activity in thermosensation.

TRPV3 in cutaneous physiology and pathophysiology

Keratinocytes are a key component of the epidermal layer and, as such, are important for the barrier function that protects skin from a variety of pathogens and damage. With the high expression of TRPV3 in keratinocytes, it is no wonder that many studies have provided insights into the involvement of TRPV3 in cutaneous homeostasis. Specifically, TRPV3 contributes to skin barrier formation, whereby moderate TRPV3 activation induces proliferation through growth factor-alpha (TGF- α)/epidermal growth factor receptor (EGFR) signaling and promotes terminal differentiation by regulating transglutaminases within skin keratinocytes^{41,42}. EGFR in turn positively regulates TRPV3 activity⁴¹. TRPV3 is also implicated in wound healing that is not confined to the skin alone^{38,43}. In addition, TRPV3 is required for hair morphogenesis or growth, which can be directly evidenced in the genetic TRPV3-knockout mice that show wavy hair and curly whiskers⁴¹. Moreover, mice with the TRPV3^{G568V} mutation exhibit a hair loss phenotype caused by premature follicular keratinocytes⁴⁴. Of particular importance here is the clinical significance of TRPV3. Many TRPV3 gain-of-function mutations (G573S, G573C, G573A, G568V, R416Q, R416W, L655P, W692S, and L694P) have been found in human patients with olmssted syndrome (OS), a hyperkeratotic skin disease^{45,46}. Among these variations, mutations at G573 and W692 tend to show more severe symptoms, and this might be attributed to mutant-TRPV3 being restricted within the ER⁴⁷. Moreover, OS patients also present with pruritus, implicating TRPV3 in itch. Although the mechanism is not fully elucidated,

in line with this, TRPV3^{G573S} DS-*Nh* mice develop dermatitis including spontaneous scratching behavior⁴⁸. Accordingly, TRPV3 levels are increased in skin biopsies of several chronic itch diseases such as AD, rosacea, and psoriasis⁴⁹⁻⁵³. Intradermal injection of carvacrol, a TRPV3 agonist, induces clear scratching behavior⁵⁴, whereas the pharmacological application of TRPV3 antagonists helps in alleviating scratching behavior in several itch models^{16,18,55}. TRPV3 activity modulates not only pruritus but also cutaneous inflammation and pain. Indeed, previously detailed skin disorders, OS, psoriasis, or AD (as well as corresponding transgenic mouse models), can sometimes result in spontaneous chronic dermatitis. Inflammation directly activates TRPV3 in keratinocytes inducing an elevated release of the mediator prostaglandin E₂ (PGE₂), ATP, or proinflammatory interleukins (IL-1 α , IL-6, or IL-8)^{56,57}. In an indirect manner, inflammatory factors induce protease-activated receptor 2 (PAR2), a GPCR, to produce thymic stromal lymphopoietin (TSLP) chemokine in keratinocytes via the TRPV3 channel⁵⁵. The notion of TRPV3 as an analgesic target was proposed based on the co-expression of TRPV3 and TRPV1 in human dorsal root ganglion (DRG) neurons, and the activation of both by noxious heat^{5,58}. Although TRPV3 is not detectable in rodent DRGs, keratinocytes are considered the primary transducer for pain via TRPV1-TRPV3 coupled signaling^{38,59}. Despite the numerous studies that have suggested roles for TRPV3 in thermosensation, barrier formation, wound healing, itching, inflammation, and pain, as mentioned above, many issues remain unclear. For example, do TRPV3 channels contribute to warmth sensation and itching directly or indirectly?

TMEM79: an emerging cutaneous target

Tmem79 was first characterized from a flaky tail mouse model commonly used in AD studies. These mice carry a frameshift mutation in the filaggrin (*Flg*) gene together with

a recessive mutation in the matted/*Tmem79* (*ma*) gene and exhibit spontaneous dermatitis, scratching, defective skin barrier, hair loss, and pulmonary inflammation phenotypes even under specific pathogen-free (SPF) conditions⁶⁰⁻⁶³. Two research groups simultaneously reported that *Tmem79*, instead of *Flg*, accounts for the spontaneous dermatitis phenotype in flaky tail mice^{61,62}. TMEM79 is a membrane protein with five transmembrane domains. It is primarily localized to the Golgi network in skin keratinocytes of the granular layer, hair follicles, prostate gland, somatosensory ganglia, and ER when overexpressed in HEK293 cells^{61,62,64-66}. Until now, very few studies have revealed the function of TMEM79. Specifically, loss of TMEM79 was shown to impair the lamellar granule secretory system, which is important for stratum corneum (SC) formation⁶¹. Furthermore, TMEM79 was proposed as a putative glutathione transferase that protects keratinocytes from oxidative stress. In this regard, the lack of TMEM79 in keratinocytes increased the level of reactive species and caused elevated PGE₂, which further modulates mast cells to release histamine and drives itch⁶⁵. It is also known that spontaneous dermatitis in *Tmem79*^{-/-} mice is associated with IL-17 driven by skin commensal, and *Il17a*^{-/-}*Tmem79*^{-/-} double knockout mice ameliorate skin inflammation and scratching behavior^{63,67}. These findings point to the possibility that skin dermatitis is inevitably caused by an impaired skin barrier. In addition to skin pathologies, TMEM79 deletion indirectly results in lung inflammation in mice, and is also required for gastrulation in *Xenopus embryos*^{63,66}. In light of the above observations, it is intriguing to further explore the potential roles of TMEM79.

Given that both TRPV3 and TMEM79 are highly expressed in skin keratinocytes, and contribute to cutaneous pathogenesis including dermatitis, skin barrier dysfunction, itching, and hair loss, I sought to understand whether TRPV3 and TMEM79 may

function together in keratinocytes. Unexpectedly, I found that TMEM79 can downregulate TRPV3-mediated activities via protein-protein interactions. Moreover, TMEM79 knockout mice prefer warmer temperatures, which is likely attributed to the increased TRPV3 levels. This finding reveals a previously unreported modulation of TRPV3 ion channels with physiological significance to thermal sensation or skin.

Materials and Methods

Animals and genotyping

Male heterozygous TMEM79 deficient (TMEM79^{+/-}) mice on a C57BL/6NCr background (Fig. S1A) were kindly provided by Dr. Takeshi Matsui and Dr. Masayuki Amagai (Laboratory for Skin Homeostasis, RIKEN, Japan). Homozygous TMEM79 deficient (TMEM79^{-/-}) mice were generated by mating male TMEM79^{+/-} and female wild-type mice for two generations. Wild-type, TMEM79^{+/-}, and TMEM79^{-/-} mice were genotyped with primers #1-3 (Table 5). The recombinant Taq™ DNA Polymerase (Takara) kit was used in a 10 µl PCR reaction with a thermal profile starting at 94°C for 2 min, followed by 35 cycles at 94°C for 15 s, 55°C for 30 s, 72°C for 30 s, and a final one min extension at 72°C. All mice were maintained under SPF conditions in a controlled environment (12 hour light/dark cycle with free access to food and water, 25°C, and 50-60% humidity). All procedures were approved by the Institutional Animal Care and Use Committee of the National Institute of Natural Sciences and carried out according to the National Institutes of Health and National Institute for Physiological Sciences guidelines.

Cell culture

Human embryonic kidney 293 (HEK293) cells were maintained at 37°C and 5% CO₂ in high glucose D-MEM culture medium (Wako) supplemented with 10% fetal bovine serum (Gibco), 2 mM GlutaMAX (Gibco), 50 units/mL penicillin, and 50 µg/mL streptomycin (Gibco). Cell passage was performed every two or three days.

DNA construction

Plasmid 3xFLAG-m*Tmem79* was generously provided by Dr. Takeshi Matsui and Dr. Masayuki Amagai. To obtain a plasmid without tags for patch-clamp, mouse *Tmem79* cDNA ([NM_024246](#)) was subcloned into the pcDNA3.1(+) vector (Invitrogen). Mouse *Trpv3* cDNA ([AF510316](#)) was cloned into the same pcDNA3.1(+) vector with or without a c-myc tag for electrophysiological or molecular experiments.

Primary mouse keratinocyte isolation and culture

Keratinocyte isolation was performed as previously described⁶⁸. Mice were first anesthetized with isoflurane then euthanized by cervical dislocation. Tails were then isolated and the skin was peeled off. The skin from each tail was dissected into four pieces and incubated with 4 mg/ml DISPASE II (Wako) in customized MCDB153 medium (CSR) containing 5 µg/mL insulin (Sigma), 0.4 µg/mL hydrocortisone (Sigma), 10 µg/mL transferrin (SCIPAC), 14.1 µg/mL phosphorylethanolamine (Sigma), 10 ng/mL epidermal growth factor (Sigma), 25 µg/mL gentamicin (Gibco), 50 units/mL penicillin, 50 µg/mL streptomycin, and 40 µg/mL bovine pituitary extracts (Kyokuto) overnight (O/N) in a cold room on a rotator. After 12-16 hours of incubation, the epidermis was detached from the dermis, and placed in 0.25% trypsin (Gibco) for 20 min at room temperature (RT) with the basal layer down. Keratinocytes were next mechanically dissociated with dissecting forceps and filtered through a 100 µm cell strainer (Falcon). The collected cells were incubated at 37°C in 5% CO₂ for further patch-clamp and molecular studies. Primary keratinocytes were maintained in the above culture medium for a maximum of one week with fresh medium replaced daily.

Transient transfection

5x10⁵ HEK293 cells were seeded onto a 3.5 cm cell culture dish (Falcon) one day before transfection. After O/N incubation at 37°C in 5% CO₂, cells were transfected with Lipofectamine reagent (Invitrogen), PLUS reagent (Invitrogen), Opti-MEM I (Gibco), and a total of 1 µg DNA at a 1:1 ratio from the paired combination of pcDNA3.1⁺ vector, (myc)-mTrpv3, or mTmem79-(3xflag) plasmids. For the patch-clamp assay and immunostaining, cells were redistributed on 12 mm micro-cover glasses (Matsunami) after three hours of incubation.

Whole-cell voltage-clamp

For HEK293 cells, patch-clamp recordings were performed within 24-30 hours after transfection. For primary skin keratinocytes, patch-clamp recordings were performed on day 2 to day 4 after isolation. A single separated cell was selected for each recording. Patch electrodes (King Precision Glass, 8250) were fabricated using a micropipette puller (Sutter, P-97) with a resistance of 4-6 MΩ. Standard extracellular 2 mM Ca²⁺ bath solution (140 mM NaCl, 5 mM KCl, 2 mM CaCl₂, 2 mM MgCl₂, 10 mM glucose, and 10 mM HEPES, pH 7.4 adjusted with NaOH) or Ca²⁺-free bath solution (140 mM NaCl, 5 mM KCl, 2 mM MgCl₂, 10 mM glucose, 5 mM EGTA, and 10 mM HEPES, PH 7.4 adjusted with NaOH) were applied for studies of physiological interactions among TRPV4/TMEM79 and TRPV3/TMEM79 in HEK293 cells, respectively. The Ca²⁺-free bath solution was also used in keratinocyte recordings. A standard intracellular pipette solution (140 mM KCl, 5 mM EGTA, and 10 mM HEPES, pH 7.4 adjusted with KOH) was utilized across all recordings. After establishing a whole-cell configuration, current was recorded from -100 mV to +100 mV voltage ramps every 3 s with a -60 mV holding potential, by applying 2-APB (Sigma) or GSK101 (Sigma) to

the bath solution. Series resistance and membrane capacitance were corrected. The data were recorded at 10 kHz (pCLAMP) and filtered at 5 kHz (Clampfit) through which current density (pA/pF) was calculated.

Ca²⁺ imaging

Primary mouse skin keratinocytes from wild-type and TMEM79^{-/-} mice were seeded onto coverslips and incubated at 37°C with fresh medium replaced daily. All recordings were performed from day 2 to day 4 after isolation. 5 μM fura-2-acetoxymethyl ester (Fura2-AM, Invitrogen) was added one hour prior to recordings. For each recording, the coverslip was washed with a standard bath solution (140 mM NaCl, 5 mM KCl, 2 mM CaCl₂, 2 mM MgCl₂, 10 mM glucose, and 10 mM HEPES, pH 7.4 adjusted with NaOH) for about one minute, and subsequently perfused with heat or chemicals followed by continuous 5 μM ionomycin (Sigma). Fura-2 AM fluorescence excited at 340 nm and 380 nm was captured every three seconds. Data were obtained and analyzed using NIS-Elements AR (Nikon) and Microsoft Excel. To compare the Ca²⁺ imaging traces from wild-type and TMEM79^{-/-} keratinocytes, all data were displayed as a normalized ratio (F340/F380) relative to ionomycin.

Co-immunoprecipitation

Twenty-four hours after transfection, HEK293 cells were gently rinsed with cold 1x PBS and collected in 600 ul RIPA buffer (Thermo Scientific) supplemented with protease inhibitor (Roche) and phosphatase inhibitor (Roche). Next, cell lysate was placed on ice for 30 min with pipetting every 10 min followed by 30 min centrifugation. The following steps were all performed at 4°C. Each supernatant sample was first cleared for 1 hour with 1 μg of off-target monoclonal IgG1 antibody produced in mouse

then transferred into 50 μ l of pre-washed Protein G Mag Sepharose bead (Cytiva) slurry for 30 min of pre-cleaning. The cell lysates were next incubated with 2 μ g of mouse anti-MYC (MBL) or mouse anti-FLAG (Sigma) O/N, and the bead pellet was discarded. On the second day, the antibody-antigen complex was precipitated with 25 μ l of fresh protein G beads for 3 hours with subsequent washing in lysis buffer three times. The complex was eventually eluted from the beads in 40 μ l of 1x sample buffer (Bio-Rad) by heating at 50°C for 10 min. 5 μ l of each sample was loaded for Western blotting. Mouse anti-MYC and rabbit anti-FLAG (FLAG; to avoid serum Ig heavy chain contamination) antibodies were used to probe for TRPV3 and TMEM79 bands, respectively.

Biotinylation of cell surface proteins

A biotinylation assay was performed in HEK293 cells 24 hours after transfection as co-IP. Cells were first washed once with PBS then gently incubated with 0.5 mg/ml EZ-Link™ Sulfo-NHS-Biotin (Thermo) twice for 10 min at 37°C. Next, the biotinylated cells were rinsed once with cold quenching buffer (100 mM glycine in PBS at pH 7.3) then washed with PBS. The cells were then collected in 200 μ l RIPA buffer supplemented with protease inhibitor and lysed on ice for 30 min with pipetting, from which 150 μ l of lysate was precipitated using 10 μ l of Dynabeads MyOne Streptavidin T1 (Invitrogen) O/N at 4°C while the remaining 50 μ l of cell lysate was used as an input sample. On the next day, the beads were denatured in 30 μ l of 1x sample buffer for 5 min at 95°C after cleaning. 4 μ l of pull-down samples and 10 μ l of input samples were electrophoresed on an 8% SDS-polyacrylamide gel. Cells transfected with empty vectors were used as a control.

Western blot

Protein samples from both HEK293 cells and primary keratinocytes were lysed in RIPA buffer with protease/phosphatase inhibitor and denatured at 95°C for 5 min or 50°C for 10 min. Equal amounts of protein were loaded and electrophoresed on 8% SDS-polyacrylamide gels for 1.5 hours at 120 V. The proteins were next transferred to a PVDF membrane in a cold room for 2 hours at 120 V. After blocking for 1 hour with BLOCK ACE (KAC) at RT, the membrane was then incubated with antibodies to detect target bands. The primary antibodies used were mouse anti-FLAG (Sigma, 1:2000), rabbit anti-FLAG (Santa Cruz, 1:1000), mouse anti-MYC (MBL, 1:1000), and HRP-conjugated anti-GAPDH (Cell Signaling, 1:1000). The secondary antibodies used were anti-mouse IgG (Cell Signaling, 1:1000) and anti-rabbit IgG (Cell Signaling, 1:1000). All proteins were incubated with an ECL kit (Cytiva), and the blots were imaged using a LAS-3000 mini (Fujifilm).

Immunofluorescence

Transfected HEK293 cells on coverslips were fixed with chilled methanol for 10 min on ice followed by three PBS washes and subsequently blocked with 10% goat serum (Sigma) for one hour at RT. The fixed cells were incubated O/N at 4°C with the following primary antibodies: rabbit anti-sodium potassium ATPase (Abcam, 1:500), mouse anti-MYC (MBL, 1:200), rabbit anti-FLAG (Santa Cruz, 1:50), mouse anti-LAMP1 (Santa Cruz, 1:100), mouse anti-Calnexin (Santa Cruz, 1:100), mouse anti-TGN38 (Invitrogen, 1:100). On the second day, cells were washed with PBS three times for 5 min each and incubated with secondary antibodies at room temperature for 1.5 hours. The following secondary antibodies were used: goat anti-mouse IgG (A-11029,

Alexa 488 conjugated, Invitrogen), goat anti-mouse IgG (A-11032, Alexa 594 conjugated, Invitrogen), goat anti-rabbit IgG (A-11034, Alexa 488 conjugated, Invitrogen), goat anti-rabbit IgG (A-11037, Alexa 594 conjugated, Invitrogen). All secondary antibodies were diluted 1:1000. The coverslips were finally mounted after incubation with DAPI (Dojindo) for 10 minutes at RT. Images were obtained using a Keyence (BZ-9000) and Olympus confocal microscope (FV3000).

Duolink proximity ligation assay

HEK293 cells were transfected with mTRPV3 alone or a combination of mTRPV3 and mTMEM79 as described above. After 24 hours, cells were fixed in 4% paraformaldehyde (PFA; Wako) for 10 min, permeabilized by PBST (0.25% triton in PBS) for 15 min at RT, and blocked with Duolink Blocking Solution (Sigma) for one hour at 37°C. Cells were next incubated with primary mouse anti-TRPV3 (Abcam, 1:200) and rabbit anti-TMEM79 (Novus, 1:200) antibodies O/N at 4°C. On the second day, cells were washed two times with buffer A (0.01 M Tris, 0.15 M NaCl, and 0.05% Tween 20, pH 7.4 adjusted with HCl), and incubated with Duolink PLA Probes anti-mouse PLUS (Sigma) and anti-rabbit MINUS (Sigma) for one hour at 37°C. Thereafter, ligation and amplification were performed with the red Duolink In Situ detection reagents kit (Sigma). Cells were then washed with buffer B (0.2 M Tris and 0.1 M NaCl, pH 7.5 adjusted with HCl) two times for 10 min each, rinsed with 0.01% buffer B for 1 min, and mounted with Duolink In Situ mounting medium with DAPI (Sigma). Images were obtained using a Keyence microscope.

RT-PCR

Total RNA was extracted from primary keratinocytes with Sepasol-RNA I Super G (Nacalai Tesque) by following the manufacturer's instructions. Sample pellets were dissolved in DEPC-treated water (Invitrogen) and quantified using a spectrophotometer (DeNovix). RNA samples (1 µg) were heated at 65°C for 5 min and subjected to reverse transcription (RT) using ReverTra Ace RT master mix (Toyobo) followed by incubation at 37°C for 15 min, 50°C for 5 min, and 98°C for 5 min. cDNA was next amplified using specific primers (Table 5 # 4-11) together with KOD Fx (Toyobo). PCR was performed under the following conditions: 94°C for 2 min, and 35 cycles at 98°C for 10 s, 55°C for 30 s, and 68°C for 40 s. Results were visualized on a 2% agarose gel.

Scratching behavior in mice

Eight-week-old male mice were used for the behavioral studies. Before recording, all mice were acclimated for 30 min in a box at set intervals to prevent mice from seeing each other. Mice were next intradermally injected with 50 µl saline or 1% carvacrol (Wako) into the right side of their neck. Scratching behaviors were subsequently captured for 1 hour using a video recorder. A single scratching bout was defined as one contact of the forepaw or hind paw at the injection site. Spontaneous scratching bouts in *TMEM79^{-/-}* mice were not counted.

Thermal behavioral assay

Intercrossed wild-type and *TMEM79^{-/-}* littermates at 7-10 weeks old were used for the thermal gradient ring (Ugo Basile) assay⁶⁹. The same background *TRPV3^{-/-}* mice were used as before²¹. All recordings were conducted between 11:00 to 20:00. The thermal

apparatus was set at a temperature gradient from 10°C to 45°C by dividing it into two identical 12-increment temperature zones at 2.9°C intervals. All animals were acclimated for 30 minutes one day prior to the experiments on a device without a thermal gradient at an ambient temperature of 25°C. All mice were released at the middle floor position followed by continuous free movement for one hour. Behaviors were individually tracked using a webcam (C920, Logitech) and transformed into processable information using ANY-maze software (Stoelting). The data were then analyzed and exported as “spent time” and “moving speed” from each specific zone using Microsoft Excel.

Results

TMEM79 reduces TRPV3-mediated currents, but not TRPV4

To examine whether TMEM79 has the ability to regulate TRPV3 activity in a heterologous system, I performed electrophysiological experiments using a whole-cell patch-clamp method in HEK293 cells transiently expressing mouse TRPV3 (mTRPV3) alone or in combination with TMEM79 (mTMEM79). Application of 300 μ M 2-APB, a TRPV3 agonist, in cells expressing both mTRPV3 and mTMEM79 (Fig. 1B, C) resulted in significantly smaller current responses than in cells expressing mTRPV3 alone (Fig. 1A, C). I next measured the currents at different concentrations of 2-APB among the two expression patterns and constructed dose-dependent curves; both TRPV3 currents activated by 2-APB showed dose-dependent activation at + 60 mV (Fig. 1D) and - 60 mV (Fig. 1E). Decreased TRPV3 currents could be attributed to either a change in dose-dependency for 2-APB or a reduction in the number of TRPV3 channels in the cells. Therefore, I evaluated the EC₅₀ values. At a voltage of + 60 mV, the mean EC₅₀ values were 57.4 ± 3.2 μ M without TMEM79 and 57.8 ± 20.8 μ M with TMEM79. At a voltage of - 60 mV, the mean EC₅₀ values were 88.3 ± 13.6 μ M without TMEM79 and 83.5 ± 18.9 μ M with TMEM79. Together, these changes in efficacy, but not potency, suggest that the difference in current amplitudes is caused by differences in the expression level of mTRPV3 in the plasma membrane.

Given the similarities between TRPV4 and TRPV3 in warmth sensitivity and localization in the skin, I also examined whether co-expression of TMEM79 could affect TRPV4-mediated currents activated by GSK101. Interestingly, TMEM79 did not alter 300 nM GSK101-induced currents (Fig. 2A-C) or currents from different

concentrations of GSK101 both at + 60 mV and – 60 mV (Fig. 2D, E), suggesting that TMEM79 specifically decreases TRPV3-evoked currents, but not TRPV4.

TMEM79 downregulates TRPV3 protein levels

I postulated above that TMEM79 reduced TRPV3 currents by regulating the protein levels of TRPV3. To address this, I performed Western blotting after labeling cell surface proteins with biotin. By overexpressing an N-terminal myc-tagged mTRPV3, a C-terminal flag-tagged mTMEM79, or transfecting both plasmids into HEK293 cells, I found that the cell surface expression and total protein levels of TRPV3 were significantly decreased by co-expression of TMEM79 (Fig. 3A, B). Among these changes, the reduction of TRPV3 protein was most predominant in the plasma membrane (Fig. 3B). Moreover, I also evaluated whether TMEM79 could affect myc-tagged TRPV3-evoked currents by performing a whole-cell patch-clamp experiment. Consistently, compared with myc-TRPV3 alone (590.8 ± 88 pA/pF at + 60 mV and 255.3 ± 61.5 pA/pF at - 60 mV, n=20), 1 mM of 2-APB induced significantly smaller TRPV3 currents with co-expression of TMEM79 both at +60 and -60 mV potentials (280 ± 58.7 pA/pF at + 60 mV and 88.2 ± 39.2 pA/pF at -60 mV, n=14; Fig. 3C), indicating that C-terminal myc-tagged mTRPV3 was likewise functionally affected by TMEM79. Together, these results demonstrate that TMEM79 decreases TRPV3-mediated currents by reducing TRPV3 expression levels mainly in the plasma membrane.

TRPV3 and TMEM79 form a complex

A physiological interaction between TRPV3 and TMEM79 implies a possible physical interaction. Therefore, I tested whether TRPV3 and TMEM79 could be

coimmunoprecipitated. Again, I transiently transfected HEK293 cells with empty pcDNA3.1⁺ vectors, myc-mTRPV3 alone, mTMEM79-flag alone, or both plasmids together. Anti-myc and anti-flag antibodies were utilized for detection of TRPV3 and TMEM79 co-IP from transfected HEK293 cells. I found that TRPV3 specifically precipitated when co-transfected cell lysates were immunoprecipitated with an anti-flag antibody, and TMEM79 was successfully immunoblotted when cell lysates were pulled down with an anti-myc antibody (Fig. 4A). Moreover, I carried out a proximity ligation assay (PLA) to confirm the physical interaction between TRPV3 and TMEM79. In the presence of both TRPV3 and TMEM79 in HEK293 cells, red punctate fluorescence was visible, indicating both proteins were in close proximity (within 40 nm; Fig. 4B). Together, these co-IP and PLA assays demonstrated that TRPV3 interacts with TMEM79 in transfected HEK293 cells.

TMEM79 alters TRPV3 localization

As discussed above, TMEM79 reduced TRPV3 expression at both the whole-cell and plasma membrane levels. I thus tested whether TMEM79 might affect the localization of TRPV3. To assess this, HEK293 cells were transfected with myc-TRPV3 plasmid or co-transfected with myc-TRPV3 and TMEM79 plasmids, then cells were immunoassayed with antibodies for myc and Na⁺/K⁺ ATPase, a membrane marker. Similar to previous reports^{30,70,71}, I found significant co-localization of TRPV3 with Na⁺/K⁺ ATPase at the plasma membrane when TRPV3 was expressed alone (Fig. 5A and B, top panels, and Fig. 5C). In contrast, co-expression of TMEM79 resulted in a broad distribution of TRPV3 in the cytoplasm (Fig. 5A and B, bottom panels, and Fig. 5C), although some TRPV3 signals remained in the plasma membrane. This observation aligned with the results obtained from the whole-cell patch-clamp

recordings and biotinylation assays, in which TMEM79 reduced TRPV3-mediated currents by decreasing TRPV3 expression in the plasma membrane. These data suggest that TMEM79 somehow mediates TRPV3 translocation.

TMEM79 restricts TRPV3 mainly in the ER and causes TRPV3 degradation in the lysosome

To further clarify the mechanisms governing the reduced TRPV3 expression in the plasma membrane, I first evaluated the intracellular localization of TRPV3 using ER and trans-Golgi organelle markers (Fig. 6A and B). Consistently, I observed high levels of TRPV3 protein in the plasma membrane with little or no localization detected with the above markers in cells expressing TRPV3 alone (Fig. 6A and B, top). In contrast, TRPV3 displayed predominant localization with the ER and little with the trans-Golgi apparatus when TMEM79 was introduced (Fig. 6A and B, bottom panel), indicating that TMEM79 restricted TRPV3 translocation in the ER, consistent with TMEM79 being an ER-resident protein as shown in a previous report⁶⁶. However, the reduced TRPV3 protein levels could be caused by either decreased synthesis or increased degradation. Given that mRNA levels in the TRPV3-transfected HEK293 cells with or without TMEM79 were unchanged (Fig. 5D), this suggests that TMEM79 is likely to promote TRPV3 degradation. Therefore, I investigated the localization of TRPV3 with a lysosomal marker, and found some TRPV3 signals overlapping with the lysosome (Fig. 6C), indicating that TMEM79 could facilitate TRPV3 degradation through a lysosomal pathway. Together, the above results demonstrate that TMEM79 is involved in the degradation and trafficking of TRPV3.

Potential interaction between TRPV4 and TMEM79

Although TMEM79 did not affect TRPV4-mediated currents (Fig. 2), I tried to determine other potential impacts related to TRPV4. Interestingly, compared with TRPV3, TMEM79 caused a different change in expression pattern for TRPV4. When TRPV4 was expressed alone, there were three bands with sizes of approximately 96, 100, and 110 kDa, while a single lowest band was observed after co-expression with TMEM79 (Fig. 7A). However, when I assessed the localization of TRPV4 within the plasma membrane, it showed an indistinguishable distribution with or without TMEM79 (Fig. 7B). Similarly, TRPV4 and TMEM79 might physically interact with each other as suggested in the PLA assay (Fig. 7C). Together, these results suggest that TMEM79 could possibly modulate TRPV4 expression instead of its physiological activities.

Keratinocytes exhibit three distinct responses to 2-APB and GSK101

TRPV3 and TRPV4, two warm-temperature sensitive TRP ion channels, are highly expressed in skin keratinocytes with suggested key roles in skin physiology and pathophysiology⁷². TMEM79 is also detected in skin keratinocytes with contributions to skin barrier formation and itch (Fig. 8A)^{61,62,65}. I therefore first examined the gene expression of *Trpv3*, *Trpv4*, and *Tmem79* by RT-PCR among skin tissues from the tail, ear, back, as well as neck, and all three genes were detectable in these tissues (Fig. 8B). Given the advantages of the hairless tail, I isolated primary keratinocytes from the tail epidermis (Fig. 8C). Afterward, I performed whole-cell patch-clamp recordings to assess the responses of primary skin keratinocytes to chemical stimuli. I applied 300 μ M of 2-APB, a TRPV3 agonist, and subsequently 1 μ M of GSK101, a TRPV4 agonist, to a single keratinocyte with a series of voltage ramps from -100 to +100 mV at a

holding potential of -60 mV (Fig. 9). Following stimulation, I characterized three types of keratinocytes from wild-type mice based on their different responses to 2-APB and GSK101 (Fig. 9A-C). Both 2-APB and GSK101 induced substantial inward and outward currents; 12.7% or 3.2% of keratinocytes showed responses to 2-APB alone or GSK 101 alone, respectively, while 84.1% of cells exhibited responses to both chemicals. This implies that most keratinocytes functionally express both TRPV3 and TRPV4.

TMEM79 regulates TRPV3-mediated currents and calcium influx in primary skin keratinocytes

From the above experiments, I concluded that TMEM79 reduces 2-APB-induced TRPV3 currents in HEK293 cells. To clarify the effects of TMEM79 in primary keratinocytes, I compared 300 μ M 2-APB-evoked and 1 μ M GSK 101-evoked currents in keratinocytes between TMEM79^{-/-} (absence of TMEM79 mRNA was confirmed, Fig. 10A) and wild-type littermate mice (Fig. 10B-D). Consistent with HEK293 cells, 300 μ M 2-APB induced significantly larger currents in TMEM79^{-/-} keratinocytes compared with wild-type, while GSK101-mediated currents did not largely differ among them. The average current densities activated by 2-APB in wild-type (Fig. 10B, top) and TMEM79^{-/-} keratinocytes (Fig. 10B, middle) were 86.8 ± 9.5 pA/pF and 160.7 ± 18.6 pA/pF at +60 mV, and 75.5 ± 6.8 pA/pF and 120.3 ± 12.4 pA/pF at -60 mV, respectively (Fig. 10D). However, the average current densities activated by GSK101 in wild-type (Fig. 10B, top) and TMEM79^{-/-} keratinocytes (Fig. 10B, middle) were 122.4 ± 10.5 pA/pF and 123.7 ± 9.6 pA/pF at +60 mV, and 64.1 ± 6.0 pA/pF and 56.7 ± 5.4 pA/pF at -60 mV, respectively (Fig. 10D). Considering that 2-APB is not a specific agonist for TRPV3, I also examined channel activity in TRPV3^{-/-} keratinocytes

(Fig. 10B, bottom). As expected, 2-APB did not elicit obvious currents whereas GSK101 induced comparable currents (166.8 ± 36.2 pA/pF at + 60 mV and 82.1 ± 19.7 pA/pF at - 60 mV) in wild-type and TMEM79^{-/-} keratinocytes, indicating that 2-APB-induced currents are derived from TRPV3 (Fig. 10D). Moreover, ratios for 2-APB-induced currents at + 100 mV to -100 mV were similar between keratinocytes from wild-type (1.18 ± 0.06 , n=15) and TMEM79^{-/-} (1.22 ± 0.06 , n=19) mice (Fig. 10E).

To further examine this, calcium imaging experiments were conducted to study TRPV3-related activity by measuring changes in intracellular calcium concentrations ($[Ca^{2+}]_i$) in Fura-2-loaded keratinocytes stimulated with heat (42°C at peak) or a TRPV3 agonist cocktail (300 μ M 2-APB and 300 μ M carvacrol), which was commonly used in previous reports^{41,50}. 5 μ M ionomycin was introduced after each stimulus for normalizing $[Ca^{2+}]_i$ values. Strikingly, $[Ca^{2+}]_i$ in individual cells was higher in keratinocytes from TMEM79^{-/-} mice compared with wild-type mice upon chemical (Fig. 11A and B) or temperature (Fig. 11C and D) stimulation confirming the increased activity of TRPV3 in TMEM79^{-/-} keratinocytes. Together, the above data corroborated that TMEM79 is required for regulating TRPV3 activity in skin keratinocytes.

TMEM79-deficient mice exhibit less scratching induced by carvacrol

Many previous studies have reported that TRPV3 activation is important in itch transmission^{54,55,73}. In particular, carvacrol, a TRPV3 agonist, induced pruritus in activating TRPV3^{18,54}. Although it is still not clear whether TRPV3 contributes to itch directly or indirectly, based on the enhanced activity in TMEM79^{-/-} keratinocytes obtained from whole-cell patch-clamp and Ca^{2+} imaging experiments (Fig. 10 and Fig. 11), I surmised that an appreciable increase in scratching induced by carvacrol would be observed in TMEM79^{-/-} mice. I, therefore, applied 1% carvacrol into the right napes

of wild-type and TMEM79^{-/-} mice by intradermal injection. However, when I analyzed the number of scratching bouts induced in one hour at the injection site, I found a pronounced reduction (approximately 70%) in frequency in TMEM79^{-/-} mice (279.7 ± 21.7 , n=11) compared with wild-type mice (81.33 ± 21.9 , n=6), which contradicted the increased TRPV3 expression in TMEM79^{-/-} mice (Fig. 12).

TMEM79-deficient mice have a pronounced alteration in temperature sensing

TRPV3 is reported to play a role in the selection of innocuous temperature, though some studies have suggested that TRPV3 has only a mild contribution to warmth perception, and effects vary amongst different genetic backgrounds or genders^{21,40}. In my study, male mice from 7 to 10 weeks of age were allowed to freely move for one hour on a Thermal Gradient (10°C to 45°C) Ring assay. The apparatus is divided into two identical 12-increment zones, with each zone representing an interval of approximately 2.9°C (Fig. 13A). “Spent time” or moving speed in each zone was recorded. Different from wild-type mice that consistently showed a moderate preference for 30°C to 35°C, I found TRPV3^{-/-} mice on a C57BL6 background exhibited a wider distribution of 25°C to 35°C (Fig. 13B, grey), which was consistent with previous studies and the latest report from our lab^{21,74}. It was also interesting that TRPV3^{-/-} mice showed a comparable occupancy as wild-type mice at both temperature zones lower than 23.1°C and higher than 37.7°C. By analyzing the exact peak temperature, we could observe that wild-type mice favored $30.4 \pm 0.5^\circ\text{C}$ (n=10) while the favored temperatures were shifted to $29.1 \pm 0.4^\circ\text{C}$ in TRPV3^{-/-} mice (n=14), demonstrating that TRPV3 is involved in warm temperature perception (Fig. 13C). Strikingly, when I examined thermal behavior in TMEM79^{-/-} mice, they displayed a more restricted distribution than wild-type and TRPV3^{-/-} mice (Fig. 13B, orange).

TMEM79^{-/-} mice spent nearly half their time in a temperature zone around 35°C with a peak at 34.4 ± 0.4°C (n=10; Fig. 13B). In addition, I also focused on the movements of mice every 20 minutes. From the data shown in Fig. 14 (A-C), it was apparent that wild-type mice started discriminating the optimal temperature after 20 minutes (Fig. 14A), while TRPV3^{-/-} mice showed an indifference to warm temperature within 40 minutes (Fig. 14B). TMEM79^{-/-} mice chose the preferred temperature within the first 20 minutes (Fig. 14C). Moreover, I evaluated the moving speed in each temperature zone since mice were expected to move slower in regions where they felt more comfortable. Consistent with their preferred temperatures, I found wild-type mice had the slowest speed in the 31.9°C to 34.8°C zones, whereas TRPV3^{-/-} and TMEM79^{-/-} mice moved slowest in the 23.1°C to 31.9°C zones and 34.8°C zone, respectively (Fig. 14D). Based on the above results, I speculated that altered thermal selection in TMEM79^{-/-} mice might be due to increased TRPV3 expression. But more direct evidence is needed to confirm the involvement of TRPV3 in the alteration of temperature preference in TMEM79^{-/-} mice.

Discussion

It had been widely debated whether itch is a sensation dependent or independent from pain because their receptors largely overlap, such as TRPV1 and TRPA1. Now we know that they are distinct sensations but interweave with each other^{75,76}. Although in recent years more and more studies are focusing on why we itch, pruritus, as an unpleasant feeling, attracts less research attention than pain. Unexpectedly, the potential importance of TRPV3 and TMEM79 first came into our focus because both proteins were suggested to be involved in itch^{61,62,65,77}. However, in my present studies, while I have yet to figure out how TRPV3 contributes to spontaneous scratching in TMEM79^{-/-} mice, I have successfully revealed the novel interplay between these membrane proteins in that TMEM79 is important for TRPV3-related electrophysiology.

In HEK293 cells, I first found that overexpression of TMEM79 could decrease TRPV3-mediated current amplitudes. This altered ion channel activity can involve fewer numbers of TRPV3 ion channels on the plasma membrane or changes to the channel properties themselves. Based on the unchanged EC₅₀ values for the 2-APB effects in TRPV3- and TRPV3/TMEM79-expressing cells, I initially believed that TMEM79 decreased TRPV3 activity by reducing TRPV3 channel protein density in the plasma membrane. This was next supported by a biotinylation assay and co-immunostaining for TRPV3 with a plasma membrane marker which demonstrated that the cell surface levels of TRPV3 protein were apparently lower when TMEM79 was introduced. Furthermore, total TRPV3 protein levels were concurrently reduced.

The aforementioned results prompted me to hypothesize that the translocation or synthesis of TRPV3 was likely affected by TMEM79. Membrane proteins are

processed in the ER, undergoing protein folding, and post-translational modifications, and are subsequently packaged into vesicles for trafficking to cell membrane⁷⁸. However, improperly folded proteins are internalized and delivered to lysosomes or proteasomes for degradation via different pathways. TRP channels are implicated in a variety of functions in almost all cell types. The translocation of TRP channels, including the thermo-TRP channels, is important for understanding how the activity of these ion channels is regulated in response to external or intracellular stimuli^{29,79}. For instance, the translocation of nociceptor TRPV1 to the cell membrane was increased by insulin and insulin growth factors (IGFs), which are required for neuronal development^{80,81}. Another study revealed that TRPV3 channels were translocated from the plasma membrane to the ER in HaCaT cells when several naturally occurring mutations were introduced at G573, as identified in OS patients, suggesting TRPV3 translocation is important in skin pathophysiology⁴⁷. With these considerations, I examined the localization of TRPV3 and found that TRPV3 displayed a clear shift from the cell surface to the cytoplasm when co-expressed with TMEM79. Based on this, I concluded that TMEM79 leads to TRPV3 becoming an ER-resident protein, and TMEM79 could promote TRPV3 degradation in the lysosome. In fact, among the thermo-TRPV channels, little is known about post-translational modifications of TRPV3. One of the few reported studies observed that sorting nexin 11 (SNX11), a vesicular trafficking protein, produced a similar outcome in TRPV3 translocation as my present study³⁰. SNX11 abolished TRPV3 trafficking to the plasma membrane and promoted TRPV3 degradation in lysosomes.

TRPV3 and TMEM79 clearly colocalized with each other when co-expressed in HEK293 cells (data not shown), which suggests both proteins likely function through

a physical interaction. By performing co-IP and PLA assays, I confirmed that TMEM79 could modulate the translocation of TRPV3 through protein-protein interactions. However, it is still not clear which regions of either protein contribute to their complex network. In terms of TRPV3, I speculate that G573 in the S4-S5 linker region may play a potential role in their interaction since mutations in this residue result in altered localization of TRPV3 as described above⁴⁷. However, future studies will be required to prove this hypothesis.

Compared with TRPV3, I observed that TMEM79 did not affect TRPV4-mediated currents or its translocation (Fig. 2 and Fig. 7B). Nevertheless, it is interesting that the three bands detected in native mTRPV4 were modified to a single band upon co-expression with TMEM79 (Fig. 7A). Several studies have reported that the multiple bands of TRPV4 are determined by N-glycosylation⁸²⁻⁸⁴. Together with a positive PLA signal between TMEM79 and TRPV4 (Fig. 7C), TMEM79 could either inhibit TRPV4 glycosylation or remove the glycans from modified TRPV4 through a protein-protein interaction. Further investigation is needed to clarify this mechanism.

Next, given the high expression of TRPV3, TRPV4, and TMEM79 in skin keratinocytes, I opted to isolate primary keratinocytes from mouse skin and perform a whole-cell patch-clamp experiment similar to that done in HEK293 cells. The functional expression of both TRPV3 and TRPV4 have been identified in previous studies^{13,18,72,85}. In this work, I newly characterized three types of keratinocytes based on their response to either 2-APB, GSK101, or both chemicals, suggesting a unique expression pattern of TRPV3 and TRPV4 in skin keratinocytes. Additionally, over 90% of keratinocytes responded to 2-APB in my experiments, which is consistent with the

high expression of TRPV3 in keratinocytes, but contradictory to several findings that only small populations of keratinocytes or HaCaT cells responded to heat or 2-APB^{30,72}. The difference between other studies and mine was that I performed a whole-cell patch-clamp experiment in a calcium-free bath solution in HEK293 cells and primary keratinocytes, while a calcium-laden bath solution was applied in most other studies. TRPV3 is unique in its sensitization by repetitive heat or chemical stimulation^{6,13,20}. Modulators such as extracellular or intracellular calcium accompanied by calmodulin could inhibit the TRPV3 channel resulting in this unique profile^{6,22}. Conversely, removal of external calcium led to increases in the initial current and population of TRPV3 by responding to stimulations of the same strength. If we consider that TMEM79 decreased the levels of cell surface TRPV3, it should lead to the same conclusion in principle whether I use a calcium-free or calcium-laden bath solution.

I next assessed the current amplitudes in keratinocytes by applying 2-APB and GSK101. Consistent with the results from HEK293 cells, larger 2-APB-induced TRPV3 currents were obtained when TMEM79 was deleted, but this was not true for TRPV4-mediated currents. These results demonstrate that TMEM79 does not affect TRPV4 membrane expression in skin keratinocytes.

In the carvacrol-induced scratching behavioral assay, I acquired a nebulous result that did not reflect the elevated TRPV3 activity in TMEM79^{-/-} keratinocytes. There might be several interpretations for this. First, I speculated that it was attributed to universal spontaneous scratching behaviors in TMEM79^{-/-} mice, which perhaps masked itching phenotypes elicited by other pruritogens, like the carvacrol applied here. Second, carvacrol is not a specific agonist for TRPV3, and could also trigger itch by activating

TRPA1^{54,73}. Thus, loss of TMEM79 might cause defective TRPA1 activity. Lastly, this phenomenon might solely reflect the real contribution of TRPV3; while TRPV3 activity was increased in TMEM79^{-/-} keratinocytes, I may not have fully accounted for the distribution of TRPV3 in other tissues. Therefore, the above irreconcilable observations may not explain the proposed interaction between TRPV3 and TMEM79 in skin keratinocytes. Nevertheless, as seen from another perspective, it is clear that more intricate mechanisms of itch underly the behavior in TMEM79^{-/-} mice.

In terms of the thermal behavioral assay, it was exhilarating to stumble upon the effect of deleting TMEM79 on mouse thermosensation. It was believed that thermal information from the skin is conveyed through the sensory nerve endings located in the epidermis to the peripheral and central nervous systems³². Recently, more *in vivo* evidence has suggested that keratinocytes are also required for perceiving temperature through temperature-sensitive ion channels³⁹. TRPV3 was suggested to be important for transmitting temperature information via keratinocytes through the release of ATP³⁷. Therefore, I speculated that TMEM79 deletion in keratinocytes increased membrane TRPV3 expression, which further induced larger currents and transmitted temperature information directly or indirectly to the central nervous system.

One previous study reported that specific overexpression of TRPV3 in mouse keratinocytes did not affect thermal selection behavior⁵⁶. Although this could refute my hypothesis, it is most likely due to the homogeneity of the genetic background of the mice. Another reason for the discrepancy could be the ring-shaped behavioral apparatus used in my study. Although I have no supportive data to demonstrate that the enhanced thermal selectivity in TMEM79^{-/-} mice is truly derived from the increased TRPV3

expression, it is reasonable to assume that TRPV3 is responsible for the altered thermal selection in TMEM79^{-/-} mice in some ways. Together with reports from others, I believe that TRPV3 in keratinocytes is not the sole protein contributing to warmth sensation, and there could be other components located downstream of keratinocytes.

Aside from warmth sensation, it is noteworthy that TRPV3 is also reported to be required in pain. Impaired responses to noxious heat have been observed in TRPV3-deficient mice²¹. Moreover, TRPV3 activation exhibits a threshold to temperatures over 50°C apart from an innocuous temperature threshold around 33°C⁸⁶. It will be meaningful to investigate pain-related phenotypes between TRPV3^{-/-} and TMEM79^{-/-} mice in the future.

A previous study proposed that TMEM79 was a putative glutathione transferase (MAPEG) that detoxified reactive oxygen species (ROS) and produced prostaglandin E2 (PGE2)⁶⁵. But to date, there has been no direct evidence to support that TMEM79 could catalyze any conjugation of glutathione or other related catalytic reactions. Although the exact biochemical function of TMEM79 remains unclear, it seems that TMEM79 is involved in post-translational modification processes based on the above described relationships between TMEM79 and TRPV3/TRPV4. This is likewise supported by a prediction in the human reference interactome (HuRI) map (<http://www.interactome-atlas.org/>) in which TMEM79 potentially interacts with a series of proteins such as E3 ubiquitin-protein ligase (RNF8), vesicle-trafficking protein (SEC22a), testis-expressed protein 264 (TEX264, which is important for ER remodeling), translocating chain-associated membrane protein 1-like 1 (TRAM1L1, which is required for translocation of proteins from ER), and stress-associated

endoplasmic reticulum protein 1 (SERP1)⁸⁷. Moreover, recent work has suggested that TMEM79 could inhibit the function of ubiquitin-specific protease 8 (USP8), a de-ubiquitinase involved in membrane trafficking pathways, which further promoted degradation and impeded the membrane trafficking of Frizzled (FZD) receptors to the cell surface⁶⁶. This implies that the same mechanism is likely to be shared in the interaction between TMEM79 and TRPV3. Related works will be needed to evaluate this hypothesis in the future.

There are some limitations to my study. First, I did not utilize mice lacking TMEM79 exclusively in keratinocytes, which may result in discrepant phenotypes in TMEM79^{-/-} mice. Second, the skin epidermal layer consists of four types of keratinocytes from the innermost to outermost layer: stratum basale, stratum spinosum, stratum granulosum, and stratum corneum⁸⁸. These cells reflect different physiological states in keratinocyte proliferation and differentiation. Although differentiation can be inhibited by eliminating calcium from the culture medium, it is hard to isolate pure keratinocytes from each layer⁸⁹. Therefore, the electrophysiological experiments performed on primary keratinocytes reflect the results of a mixed pool. Lastly, because of the ineffective performance of the TRPV3 antibodies in my hands, I am currently unable to confirm an increase in TRPV3 protein levels in TMEM79-deficient keratinocytes or the physical interaction between TRPV3 and TMEM79 in primary cells using a protein assay. Overall, however, the interaction between TRPV3 and TMEM79 provides us with a new model which may be important for skin homeostasis or thermoregulation.

References

1. Cosens, D. J. & Manning, A. Abnormal Electroretinogram from a *Drosophila* Mutant. *Nature* **224**, 285–287 (1969).
2. Montell, C. & Rubin, G. M. Molecular characterization of the *drosophila* *trp* locus: A putative integral membrane protein required for phototransduction. *Neuron* **2**, 1313–1323 (1989).
3. Zheng, J. Molecular Mechanism of TRP Channels. *Compr. Physiol.* **3**, 221–242 (2013).
4. Nilius, B. & Owsianik, G. The transient receptor potential family of ion channels. *Genome Biol.* **12**, 218 (2011).
5. Smith, G. D. *et al.* TRPV3 is a temperature-sensitive vanilloid receptor-like protein. *Nature* **418**, 186–190 (2002).
6. Peier, A. M. *et al.* A Heat-Sensitive TRP Channel Expressed in Keratinocytes. *Science* **296**, 2046–2049 (2002).
7. Ueda, T., Yamada, T., Ugawa, S., Ishida, Y. & Shimada, S. TRPV3, a thermosensitive channel is expressed in mouse distal colon epithelium. *Biochem. Biophys. Res. Commun.* **383**, 130–134 (2009).
8. Xu, H., Delling, M., Jun, J. C. & Clapham, D. E. Oregano, thyme and clove-derived flavors and skin sensitizers activate specific TRP channels. *Nat. Neurosci.* **9**, 628–635 (2006).
9. Yamada, T. *et al.* Functional expression of transient receptor potential vanilloid 3 (TRPV3) in corneal epithelial cells: Involvement in thermosensation and wound healing. *Exp. Eye Res.* **90**, 121–129 (2010).

10. Burrell, K. L. *et al.* Dynamic Expression of TRPV3 and Integrated Signaling with Growth Factor Pathways During Lung Epithelial Wound Repair Following Wood Smoke Particle and Other Forms of Lung Cell Injury. *Mol. Pharmacol.* (2021).
11. Nilius, B., Bíró, T. & Owsianik, G. TRPV3: time to decipher a poorly understood family member! *J. Physiol.* **592**, 295–304 (2014).
12. Vogt-Eisele, A. K. *et al.* Monoterpenoid agonists of TRPV3. *Br. J. Pharmacol.* **151**, 530–540 (2007).
13. Chung, M.-K., Lee, H., Mizuno, A., Suzuki, M. & Caterina, M. J. 2-Aminoethoxydiphenyl Borate Activates and Sensitizes the Heat-Gated Ion Channel TRPV3. *J. Neurosci.* **24**, 5177–5182 (2004).
14. Singh, A. K., McGoldrick, L. L. & Sobolevsky, A. I. Structure and Gating Mechanism of the Transient Receptor Potential Channel TRPV3. *Nat. Struct. Mol. Biol.* **25**, 805 (2018).
15. Hu, H., Grandl, J., Bandell, M., Petrus, M. & Patapoutian, A. Two amino acid residues determine 2-APB sensitivity of the ion channels TRPV3 and TRPV4. *Proc. Natl. Acad. Sci.* **106**, 1626–1631 (2009).
16. Han, Y. *et al.* A plant-derived TRPV3 inhibitor suppresses pain and itch. *Br. J. Pharmacol.* **178**, 1669–1683 (2021).
17. Structural mechanism of TRPV3 channel inhibition by the plant-derived coumarin osthole. *EMBO Rep.* **22**, e53233 (2021).
18. Liu, Q. *et al.* Therapeutic inhibition of keratinocyte TRPV3 sensory channel by local anesthetic dyclonine. *eLife* **10**, e68128 (2021).

19. Neuberger, A., Nadezhdin, K. D. & Sobolevsky, A. I. Structural mechanism of TRPV3 channel inhibition by the anesthetic dyclonine. *Nat. Commun.* **13**, 2795 (2022).
20. Liu, B., Yao, J., Zhu, M. X. & Qin, F. Hysteresis of gating underlines sensitization of TRPV3 channels. *J. Gen. Physiol.* **138**, 509–520 (2011).
21. Moqrich, A. *et al.* Impaired Thermosensation in Mice Lacking TRPV3, a Heat and Camphor Sensor in the Skin. *Science* **307**, 1468–1472 (2005).
22. Xiao, R. *et al.* Calcium Plays a Central Role in the Sensitization of TRPV3 Channel to Repetitive Stimulations *. *J. Biol. Chem.* **283**, 6162–6174 (2008).
23. Phelps, C. B., Wang, R. R., Choo, S. S. & Gaudet, R. Differential Regulation of TRPV1, TRPV3, and TRPV4 Sensitivity through a Conserved Binding Site on the Ankyrin Repeat Domain *. *J. Biol. Chem.* **285**, 731–740 (2010).
24. Wang, H. *et al.* Mechanisms of proton inhibition and sensitization of the cation channel TRPV3. *J. Gen. Physiol.* **153**, (2021).
25. Gao, L. *et al.* Selective potentiation of 2-APB-induced activation of TRPV1–3 channels by acid. *Sci. Rep.* **6**, 20791 (2016).
26. HU, H.-Z. *et al.* Potentiation of TRPV3 Channel Function by Unsaturated Fatty Acids. *J. Cell. Physiol.* **208**, 201–212 (2006).
27. Doerner, J. F., Hatt, H. & Ramsey, I. S. Voltage- and temperature-dependent activation of TRPV3 channels is potentiated by receptor-mediated PI(4,5)P₂ hydrolysis. *J. Gen. Physiol.* **137**, 271–288 (2011).
28. Luo, J., Stewart, R., Berdeaux, R. & Hu, H. Tonic Inhibition of TRPV3 by Mg²⁺ in Mouse Epidermal Keratinocytes. *J. Invest. Dermatol.* **132**, 2158–2165 (2012).

29. Ferrandiz-Huertas, C., Mathivanan, S., Wolf, C. J., Devesa, I. & Ferrer-Montiel, A. Trafficking of ThermoTRP Channels. *Membranes* **4**, 525–564 (2014).
30. Li, C. *et al.* Sorting Nexin 11 Regulates Lysosomal Degradation of Plasma Membrane TRPV3. *Traffic* **17**, 500–514 (2016).
31. Caterina, M. J. *et al.* The capsaicin receptor: a heat-activated ion channel in the pain pathway. *Nature* **389**, 816–824 (1997).
32. Vriens, J., Nilius, B. & Voets, T. Peripheral thermosensation in mammals. *Nat. Rev. Neurosci.* **15**, 573–589 (2014).
33. Caterina, M. J. *et al.* Impaired Nociception and Pain Sensation in Mice Lacking the Capsaicin Receptor. *Science* (2000) doi:10.1126/science.288.5464.306.
34. Vandewauw, I. *et al.* A TRP channel trio mediates acute noxious heat sensing. *Nature* **555**, 662–666 (2018).
35. Bautista, D. M. *et al.* The menthol receptor TRPM8 is the principal detector of environmental cold. *Nature* **448**, 204–208 (2007).
36. Lee, H., Iida, T., Mizuno, A., Suzuki, M. & Caterina, M. J. Altered Thermal Selection Behavior in Mice Lacking Transient Receptor Potential Vanilloid 4. *J. Neurosci.* **25**, 1304–1310 (2005).
37. Mandadi, S. *et al.* TRPV3 in keratinocytes transmits temperature information to sensory neurons via ATP. *Pflugers Arch.* **458**, 1093–1102 (2009).
38. Miyamoto, T., Petrus, M. J., Dubin, A. E. & Patapoutian, A. TRPV3 regulates nitric oxide synthase-independent nitric oxide synthesis in the skin. *Nat. Commun.* **2**, 369 (2011).
39. Sadler, K. E., Moehring, F. & Stucky, C. L. Keratinocytes contribute to normal cold and heat sensation. *eLife* **9**, e58625 (2020).

40. Huang, S. M., Li, X., Yu, Y., Wang, J. & Caterina, M. J. TRPV3 and TRPV4 Ion Channels are Not Major Contributors to Mouse Heat Sensation. *Mol. Pain* **7**, 1744-8069-7–37 (2011).
41. Cheng, X. *et al.* TRP Channel Regulates EGFR Signaling in Hair Morphogenesis and Skin Barrier Formation. *Cell* **141**, 331–343 (2010).
42. Wang, Y. *et al.* TRPV3 enhances skin keratinocyte proliferation through EGFR-dependent signaling pathways. *Cell Biol. Toxicol.* **37**, 313–330 (2021).
43. Aijima, R. *et al.* The thermosensitive TRPV3 channel contributes to rapid wound healing in oral epithelia. *FASEB J.* **29**, 182–192 (2015).
44. Song, Z. *et al.* Hair Loss Caused by Gain-of-Function Mutant TRPV3 Is Associated with Premature Differentiation of Follicular Keratinocytes. *J. Invest. Dermatol.* **141**, 1964–1974 (2021).
45. Zhong, W. *et al.* Genotype–Phenotype Correlation of TRPV3-Related Olmsted Syndrome. *J. Invest. Dermatol.* **141**, 545–554 (2021).
46. Lin, Z. *et al.* Exome Sequencing Reveals Mutations in TRPV3 as a Cause of Olmsted Syndrome. *Am. J. Hum. Genet.* **90**, 558–564 (2012).
47. Yadav, M. & Goswami, C. TRPV3 mutants causing Olmsted Syndrome induce impaired cell adhesion and nonfunctional lysosomes. *Channels* **11**, 196–208 (2016).
48. Yoshioka, T. *et al.* Impact of the Gly573Ser Substitution in TRPV3 on the Development of Allergic and Pruritic Dermatitis in Mice. *J. Invest. Dermatol.* **129**, 714–722 (2009).
49. Yamamoto-Kasai, E., Yasui, K., Shichijo, M., Sakata, T. & Yoshioka, T. Impact of TRPV3 on the development of allergic dermatitis as a dendritic cell modulator. *Exp. Dermatol.* **22**, 820–824 (2013).

50. Seo, S. H., Kim, S., Kim, S.-E., Chung, S. & Lee, S. E. Enhanced Thermal Sensitivity of TRPV3 in Keratinocytes Underlies Heat-Induced Pruritogen Release and Pruritus in Atopic Dermatitis. *J. Invest. Dermatol.* **140**, 2199-2209.e6 (2020).
51. Larkin, C. *et al.* Novel insights into the TRPV3-mediated itch in atopic dermatitis. *J. Allergy Clin. Immunol.* **147**, 1110-1114.e5 (2021).
52. Sulk, M. *et al.* Distribution and Expression of Non-Neuronal Transient Receptor Potential (TRPV) Ion Channels in Rosacea. *J. Invest. Dermatol.* **132**, 1253–1262 (2012).
53. Nattkemper, L. A. *et al.* The Genetics of Chronic Itch: Gene Expression in the Skin of Patients with Atopic Dermatitis and Psoriasis with Severe Itch. *J. Invest. Dermatol.* **138**, 1311–1317 (2018).
54. Cui, T., Wang, G., Wei, N. & Wang, K. A pivotal role for the activation of TRPV3 channel in itch sensations induced by the natural skin sensitizer carvacrol. *Acta Pharmacol. Sin.* **39**, 331–335 (2018).
55. Zhao, J. *et al.* PAR2 Mediates Itch via TRPV3 Signaling in Keratinocytes. *J. Invest. Dermatol.* **140**, 1524–1532 (2020).
56. Huang, S. M. *et al.* Overexpressed Transient Receptor Potential Vanilloid 3 Ion Channels in Skin Keratinocytes Modulate Pain Sensitivity via Prostaglandin E2. *J. Neurosci.* **28**, 13727–13737 (2008).
57. Szöllősi, A. G. *et al.* Activation of TRPV3 Regulates Inflammatory Actions of Human Epidermal Keratinocytes. *J. Invest. Dermatol.* **138**, 365–374 (2018).
58. Facer, P. *et al.* Differential expression of the capsaicin receptor TRPV1 and related novel receptors TRPV3, TRPV4 and TRPM8 in normal human tissues and changes in traumatic and diabetic neuropathy. *BMC Neurol.* **7**, 11 (2007).

59. Martin, L. S., Fraillon, E., Chevalier, F. P. & Fromy, B. *Hot on the Trail of Skin Inflammation: Focus on TRPV1/TRPV3 Channels in Psoriasis*. (IntechOpen, 2022). doi:10.5772/intechopen.103792.
60. Fallon, P. G. *et al.* A homozygous frameshift mutation in the mouse Flg gene facilitates enhanced percutaneous allergen priming. *Nat. Genet.* **41**, 602–608 (2009).
61. Sasaki, T. *et al.* A homozygous nonsense mutation in the gene for Tmem79, a component for the lamellar granule secretory system, produces spontaneous eczema in an experimental model of atopic dermatitis. *J. Allergy Clin. Immunol.* **132**, 1111-1120.e4 (2013).
62. Saunders, S. P. *et al.* Tmem79/Matt is the matted mouse gene and is a predisposing gene for atopic dermatitis in human subjects. *J. Allergy Clin. Immunol.* **132**, 1121–1129 (2013).
63. Saunders, S. P. *et al.* Dysregulated skin barrier function in Tmem79 mutant mice promotes IL-17A-dependent spontaneous skin and lung inflammation. *Allergy* **75**, 3216–3227 (2020).
64. O’Hurley, G. *et al.* Analysis of the Human Prostate-Specific Proteome Defined by Transcriptomics and Antibody-Based Profiling Identifies TMEM79 and ACOXL as Two Putative, Diagnostic Markers in Prostate Cancer. *PLOS ONE* **10**, e0133449 (2015).
65. Emrick, J. J. *et al.* Tissue-specific contributions of Tmem79 to atopic dermatitis and mast cell-mediated histaminergic itch. *Proc. Natl. Acad. Sci.* **115**, E12091–E12100 (2018).

66. Chen, M. *et al.* TMEM79/MATTRIN defines a pathway for Frizzled regulation and is required for *Xenopus* embryogenesis. *eLife* **9**, e56793 (2020).
67. Ito, Y. *et al.* *Staphylococcus cohnii* is a potentially biotherapeutic skin commensal alleviating skin inflammation. *Cell Rep.* **35**, 109052 (2021).
68. Li, F., Adase, C. A. & Zhang, L. Isolation and Culture of Primary Mouse Keratinocytes from Neonatal and Adult Mouse Skin. *J. Vis. Exp. JoVE* 56027 (2017) doi:10.3791/56027.
69. Touska, F. *et al.* Comprehensive thermal preference phenotyping in mice using a novel automated circular gradient assay. *Temperature* **3**, 77–91 (2016).
70. Liebe, H., Liebe, F., Sponder, G., Hedtrich, S. & Stumpff, F. Beyond Ca²⁺ signalling: the role of TRPV3 in the transport of NH₄⁺. *Pflüg. Arch. - Eur. J. Physiol.* **473**, 1859–1884 (2021).
71. Hellwig, N., Albrecht, N., Harteneck, C., Schultz, G. & Schaefer, M. Homo- and heteromeric assembly of TRPV channel subunits. *J. Cell Sci.* **118**, 917–928 (2005).
72. Chung, M.-K., Lee, H., Mizuno, A., Suzuki, M. & Caterina, M. J. TRPV3 and TRPV4 Mediate Warmth-evoked Currents in Primary Mouse Keratinocytes *. *J. Biol. Chem.* **279**, 21569–21575 (2004).
73. Kittaka, H. & Tominaga, M. The molecular and cellular mechanisms of itch and the involvement of TRP channels in the peripheral sensory nervous system and skin. *Allergol. Int.* **66**, 22–30 (2017).
74. Ujisawa, T., Sasajima, S., Kashio, M. & Tominaga, M. Thermal gradient ring reveals different temperature-dependent behaviors in mice lacking thermosensitive TRP channels. *J. Physiol. Sci.* **72**, 11 (2022).

75. Liu, T. & Ji, R.-R. New insights into the mechanisms of itch: are pain and itch controlled by distinct mechanisms? *Pflugers Arch.* **465**, 10.1007/s00424-013-1284-2 (2013).
76. Dong, X. & Dong, X. Peripheral and Central Mechanisms of Itch. *Neuron* **98**, 482–494 (2018).
77. Wang, G. & Wang, K. The Ca²⁺-Permeable Cation Transient Receptor Potential TRPV3 Channel: An Emerging Pivotal Target for Itch and Skin Diseases. *Mol. Pharmacol.* **92**, 193–200 (2017).
78. Alberts, B. *et al.* *Molecular Biology of the Cell.* (Garland Science, 2002).
79. R, P.-C. & A, F.-M. TRP Channel Trafficking. (2011).
80. Van Buren, J. J., Bhat, S., Rotello, R., Pauza, M. E. & Premkumar, L. S. Sensitization and translocation of TRPV1 by insulin and IGF-I. *Mol. Pain* **1**, 17 (2005).
81. Lewitt, M. S. & Boyd, G. W. The Role of Insulin-Like Growth Factors and Insulin-Like Growth Factor–Binding Proteins in the Nervous System. *Biochem. Insights* **12**, 1178626419842176 (2019).
82. Xu, H., Fu, Y., Tian, W. & Cohen, D. M. Glycosylation of the osmosensitive transient receptor potential channel TRPV4 on Asn-651 influences membrane trafficking. *Am. J. Physiol.-Ren. Physiol.* **290**, F1103–F1109 (2006).
83. Arniges, M., Fernández-Fernández, J. M., Albrecht, N., Schaefer, M. & Valverde, M. A. Human TRPV4 Channel Splice Variants Revealed a Key Role of Ankyrin Domains in Multimerization and Trafficking*. *J. Biol. Chem.* **281**, 1580–1586 (2006).
84. Lamandé, S. R. *et al.* Mutations in TRPV4 cause an inherited arthropathy of hands and feet. *Nat. Genet.* **43**, 1142–1146 (2011).

85. Luo, J. *et al.* Transient receptor potential vanilloid 4–expressing macrophages and keratinocytes contribute differentially to allergic and nonallergic chronic itch. *J. Allergy Clin. Immunol.* **141**, 608-619.e7 (2018).
86. Liu, B. & Qin, F. Single-residue molecular switch for high-temperature dependence of vanilloid receptor TRPV3. *Proc. Natl. Acad. Sci.* **114**, 1589–1594 (2017).
87. Luck, K. *et al.* A reference map of the human binary protein interactome. *Nature* **580**, 402–408 (2020).
88. Matsui, T. & Amagai, M. Dissecting the formation, structure and barrier function of the stratum corneum. *Int. Immunol.* **27**, 269–280 (2015).
89. Tu, C.-L., Oda, Y., Komuves, L. & Bikle, D. D. The role of the calcium-sensing receptor in epidermal differentiation. *Cell Calcium* **35**, 265–273 (2004).

Figures

Figure 1

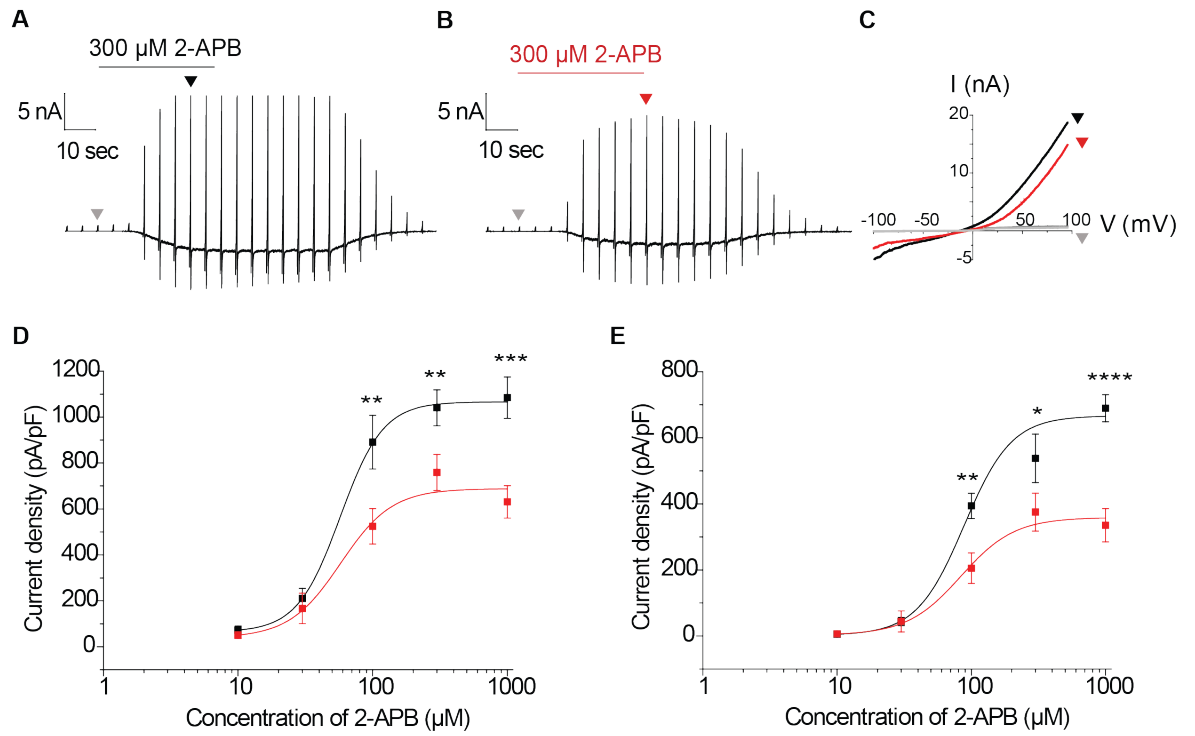


Figure 1

TMEM79 reduces the 2-APB-induced TRPV3 current amplitudes in HEK293 cells

(A and B) Representative 2-APB-evoked (300 μ M) current traces in a mTRPV3-transfected HEK293 cell (A) and a mTRPV3/mTMEM79-transfected HEK293 cell (B). Recordings were performed in a ramp-pulse protocol (-100 to +100 mV) every three seconds at a holding potential of -60 mV. Scale bars indicate current amplitudes (y-axis, nA) and time (x-axis, sec). (C) I-V curves from the pulses are shown in grey, black, and red. (D and E) 2-APB dose-dependent curves in HEK293 cells transfected with mTRPV3 alone (black) or co-transfected with mTRPV3 and mTMEM79 (red) at +60 mV (D) and -60 mV (E). The EC_{50} was $57.4 \pm 3.2 \mu$ M (black) and $57.8 \pm 20.8 \mu$ M (red) at +60 mV, and $88.3 \pm 13.6 \mu$ M (black) and $83.5 \pm 18.9 \mu$ M (red) at -60 mV. Current densities (pA/pF) represent the largest values of the 2-APB-induced currents. Number of recordings: n=4-23. All curves were fitted with the Hill equation with a Hill coefficient (n) around 2. Statistics were performed by a one-tailed unpaired t-test. All error bars and data represent the mean \pm SEM. * $P \leq 0.05$, ** $P \leq 0.01$, *** $P \leq 0.001$, **** $P \leq 0.0001$.

Figure 2

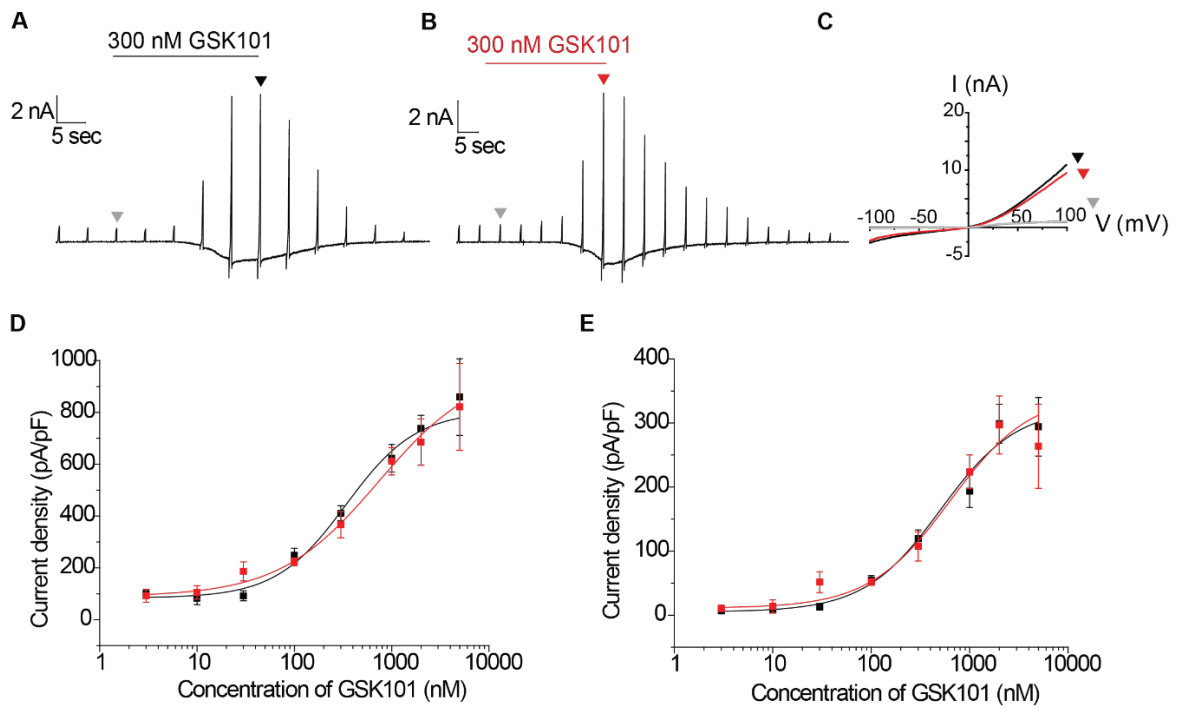


Figure 2

TMEM79 does not affect the GSK101-induced TRPV4 current amplitudes in HEK293 cells

(A and B) Representative GSK101-evoked (300 nM) current traces in a mTRPV4-transfected HEK293 cell (A) and a mTRPV4/mTMEM79-transfected HEK293 cell (B). Recordings were performed in a ramp-pulse protocol (-100 to +100 mV) every three seconds at a holding potential of -60 mV. Scale bars indicate current amplitudes (y-axis, nA) and time (x-axis, sec). (C) I-V curves from the pulses are shown in grey, black, and red. (D and E) GSK101 dose-dependent curves in HEK293 cells transfected with mTRPV4 alone (black) or cotransfected with mTRPV4 and mTMEM79 (red) at +60 mV (D) and -60 mV (E). Current densities (pA/pF) represent the largest values of the GSK101-induced currents. Number of recordings: n=4-15. All curves were fitted with the Hill equation with a Hill coefficient (n) around 1. Statistics were performed by a two-tailed unpaired t-test. All error bars and data represent the mean \pm SEM.

Figure 3

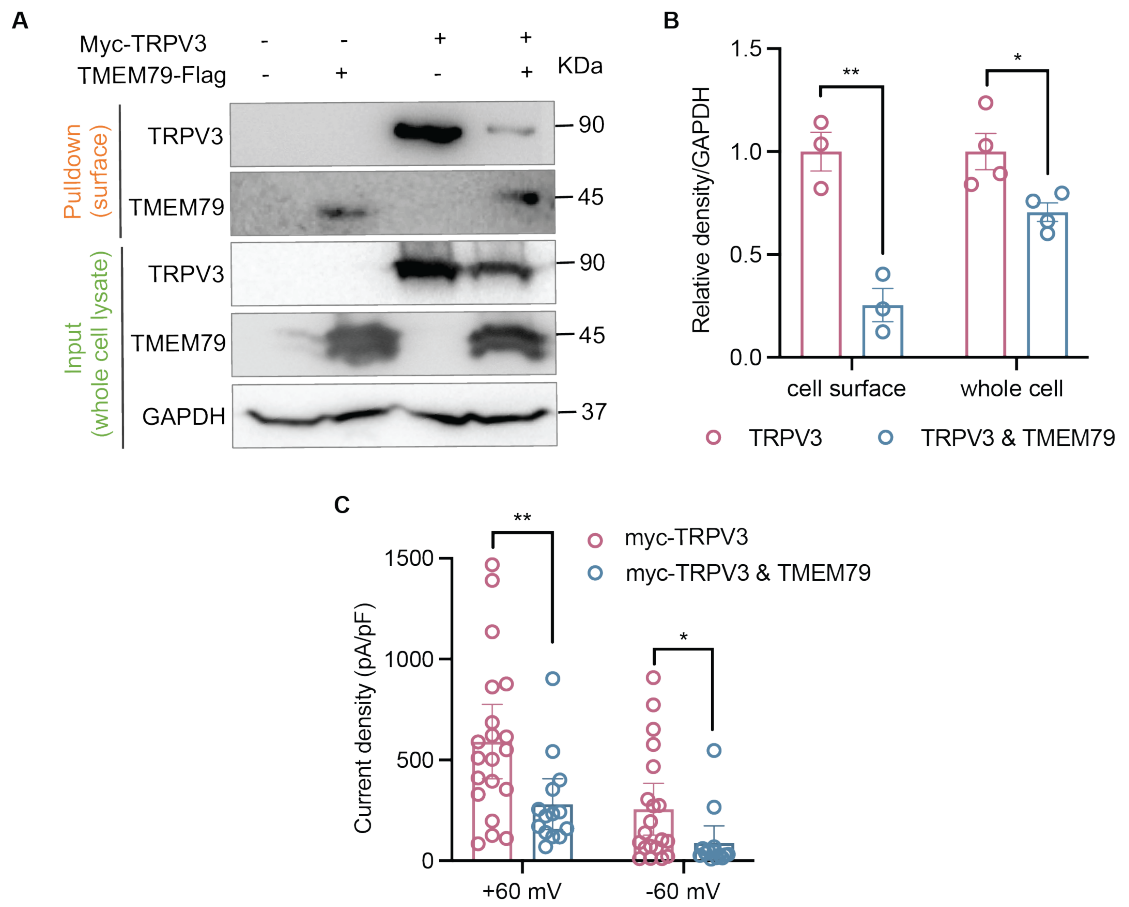


Figure 3

TMEM79 down-regulates TRPV3 protein levels predominantly in the plasma membrane

(A) HEK293 cells transiently transfected with empty vectors, myc-mTRPV3 alone, mTMEM79-flag alone, or both myc-mTRPV3 and mTMEM79-flag were biotinylated and immunoblotted with antibodies against the myc-tag and flag-tag at both the cell surface (pulldown) and whole-cell lysate (input) levels. (B) Quantitative analysis of the normalized band densities of TRPV3 to GAPDH in HEK293 cells expressing myc-mTRPV3 alone (red circles) or co-expressing myc-mTRPV3 and mTMEM79-flag (blue circles) in the plasma membrane (n=3) and whole-cell lysates (n=4). (C) Comparison of 1 mM 2-APB-induced current densities in HEK293 cells expressing myc-mTRPV3 (red circles, 590.8 ± 88 pA/pF at + 60 mV and 255.3 ± 61.5 pA/pF at - 60 mV, n=20) or both myc-mTRPV3 and mTMEM79 (blue circles, 280 ± 58.7 pA/pF at + 60 mV and 88.2 ± 39.2 pA/pF at -60 mV, n=14) at ± 60 mV. Statistics were performed by a one-tailed unpaired t-test. All data represent the mean \pm SEM and all error bars indicate a 95% confidence interval for the mean. * $P \leq 0.05$, ** $P \leq 0.01$.

Figure 4

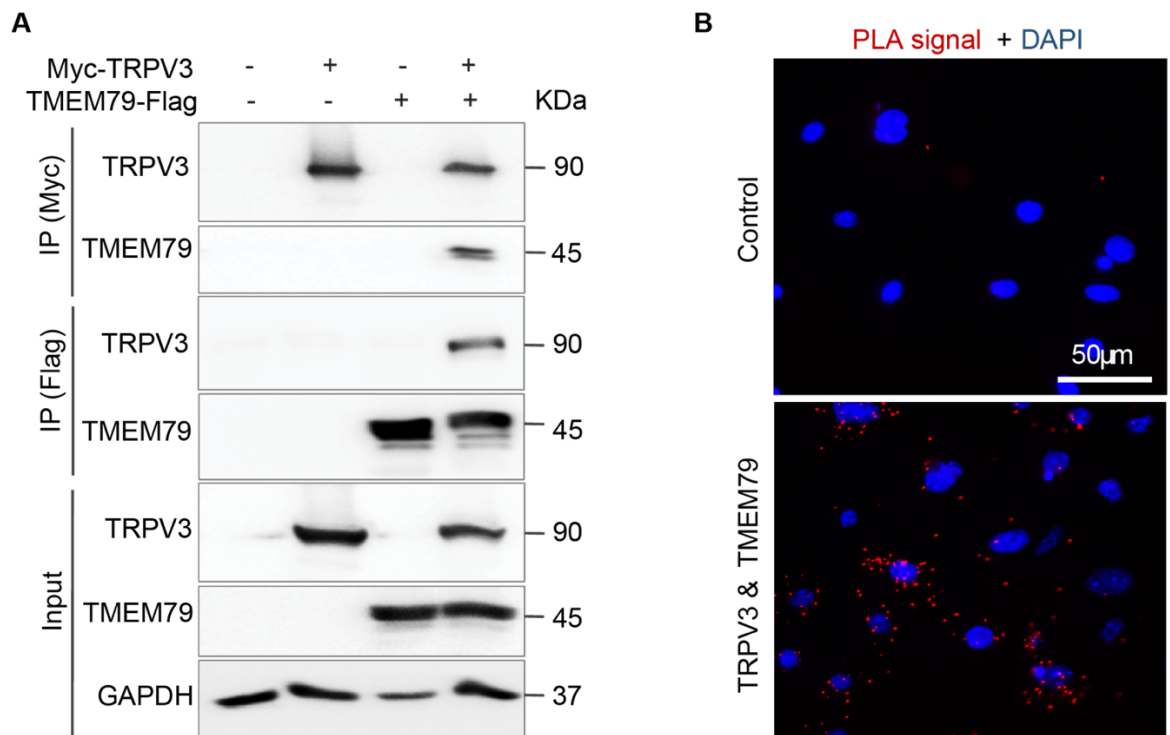


Figure 4

TRPV3 and TMEM79 bind to each other

(A) Coimmunoprecipitation (co-IP) of TRPV3 and TMEM79 in HEK293 cells. HEK293 cells transiently transfected with empty vectors, myc-mTRPV3 alone, mTMEM79-flag alone, or both myc-mTRPV3 and mTMEM79-flag were immunoprecipitated with anti-myc or anti-flag antibodies. Bands were detected using antibodies against the myc-tag and flag-tag by avoiding the IgG heavy chain around 50 kDa. Input immunoblots indicate TRPV3, TMEM79, as well as GAPDH bands in the whole-cell lysates before co-IP. The proteins were detected by ECL. (B) Representative images of the PLA assay in HEK293 cells. HEK293 cells transfected with empty vectors (control) or mTRPV3/mTMEM79 were assayed using antibodies against TRPV3 and TMEM79. The PLA probes used were anti-mouse PLUS and anti-rabbit MINUS. Red puncta indicate the sites of interaction between TRPV3 and TMEM79 in HEK293 cells. Nuclei were stained with DAPI, shown in blue. Scale bars indicate 50 μm .

Figure 5

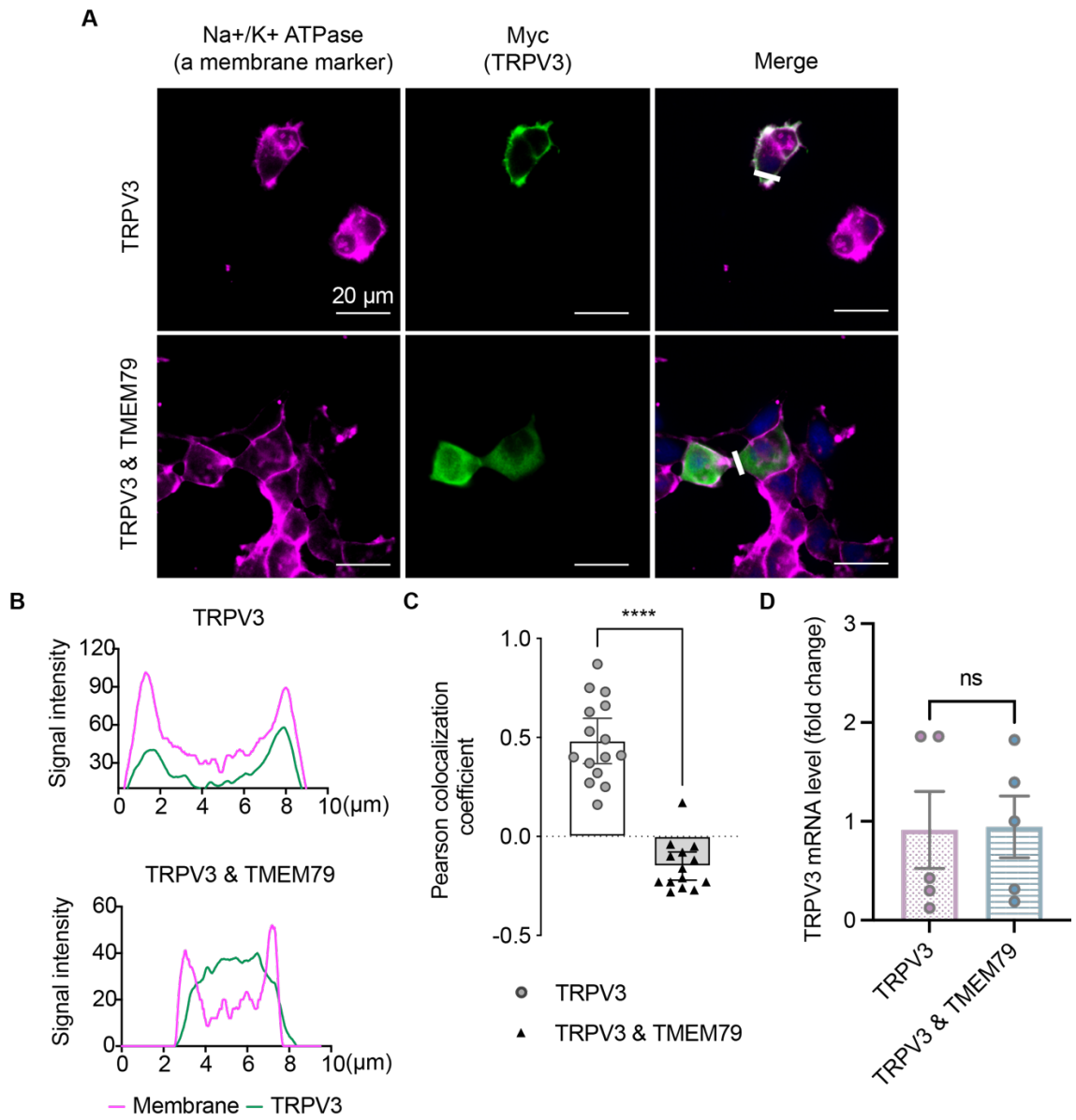


Figure 5

TMEM79 alters the localization of TRPV3 in HEK293 cells

(A) Immunofluorescence images of TRPV3 localization. HEK293 cells transiently transfected with myc-mTRPV3 alone, or both myc-mTRPV3 and mTMEM79-flag were stained with antibodies against Na⁺/K⁺ ATPase (magenta) and myc-tag (green). Nuclei were stained with DAPI (blue). Myc-mTRPV3 alone clearly localizes with Na⁺/K⁺ ATPase (a cell membrane marker), while it displays cytoplasmic retention after the administration of mTMEM79. Scale bars indicate 20 μm. (B) Signal intensities of the TRPV3 signal alone are indicated by the white line in each representative merged image in (A). (C) Quantification of Pearson colocalization coefficient between TRPV3 and Na⁺/K⁺ ATPase. The ROIs representing 1-3 cells were analyzed together using the Coloc 2 plugin in Fiji. Pearson's R-value is 0.48 ± 0.05 in HEK293 cells expressing TRPV3 (n=15) and -0.15 ± 0.03 in HEK293 cells expressing TRPV3/TMEM79 (n=14). (D) TRPV3 mRNA levels in HEK293 cells expressing TRPV3 or TRPV3/TMEM79. Statistics were performed by a two-tailed unpaired t-test. All data represent the mean \pm SEM and all error bars indicate a 95% confidence interval for the mean. **** $P \leq 0.0001$, ns, $P > 0.05$.

Figure 6

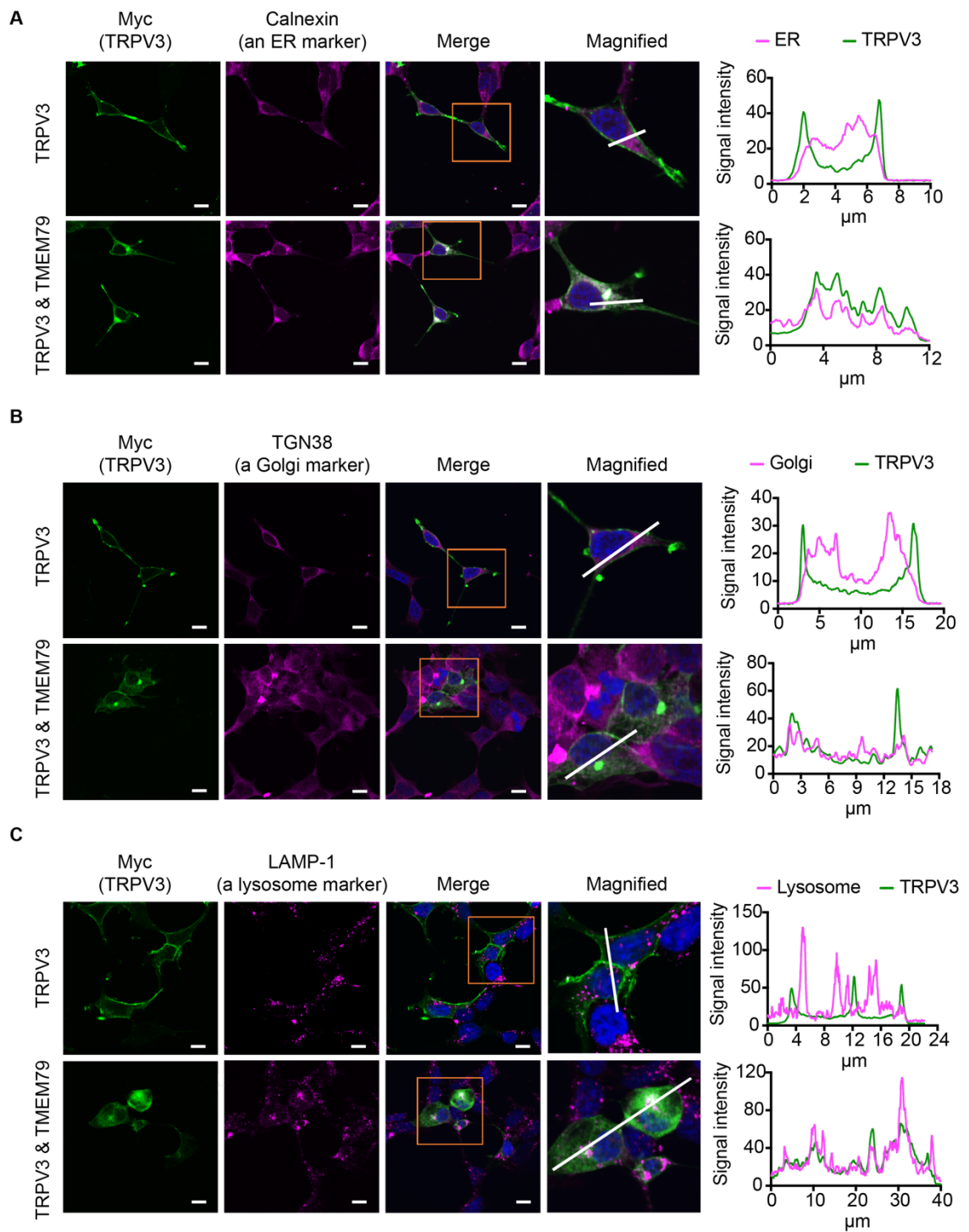


Figure 6

Subcellular localization of TRPV3 in HEK293 cells

(A, B, and C) Immunofluorescence images of TRPV3 (green) with markers of the ER, trans-Golgi, and lysosome (magenta), respectively. Nuclei were stained with DAPI (blue). HEK293 cells transiently transfected with myc-mTRPV3 alone or both myc-mTRPV3 and mTMEM79 were co-stained with an antibody against the myc-tag together with antibodies against Calnexin (A), TGN38 (B), and LAMP-1 (C). TRPV3 alone did not show clear localization within the three organelles. However, with co-expression of TMEM79, (A) TRPV3 signals clearly overlapped with the ER marker suggesting TRPV3 was mainly localized to the ER. (B) There were few overlapping signals between TRPV3 and the trans-Golgi marker indicating TRPV3 was likely restricted in its translocation from the trans-Golgi to plasma membrane. (C) TRPV3 exhibited moderate colocalization with the lysosome marker indicating some involvement of TRPV3 in the lysosomal degradation pathway. The orange boxed areas are shown magnified and signals from the white solid lines are graphed in the right panels as fluorescence intensity. All scale bars indicate 10 μ m.

Figure 7

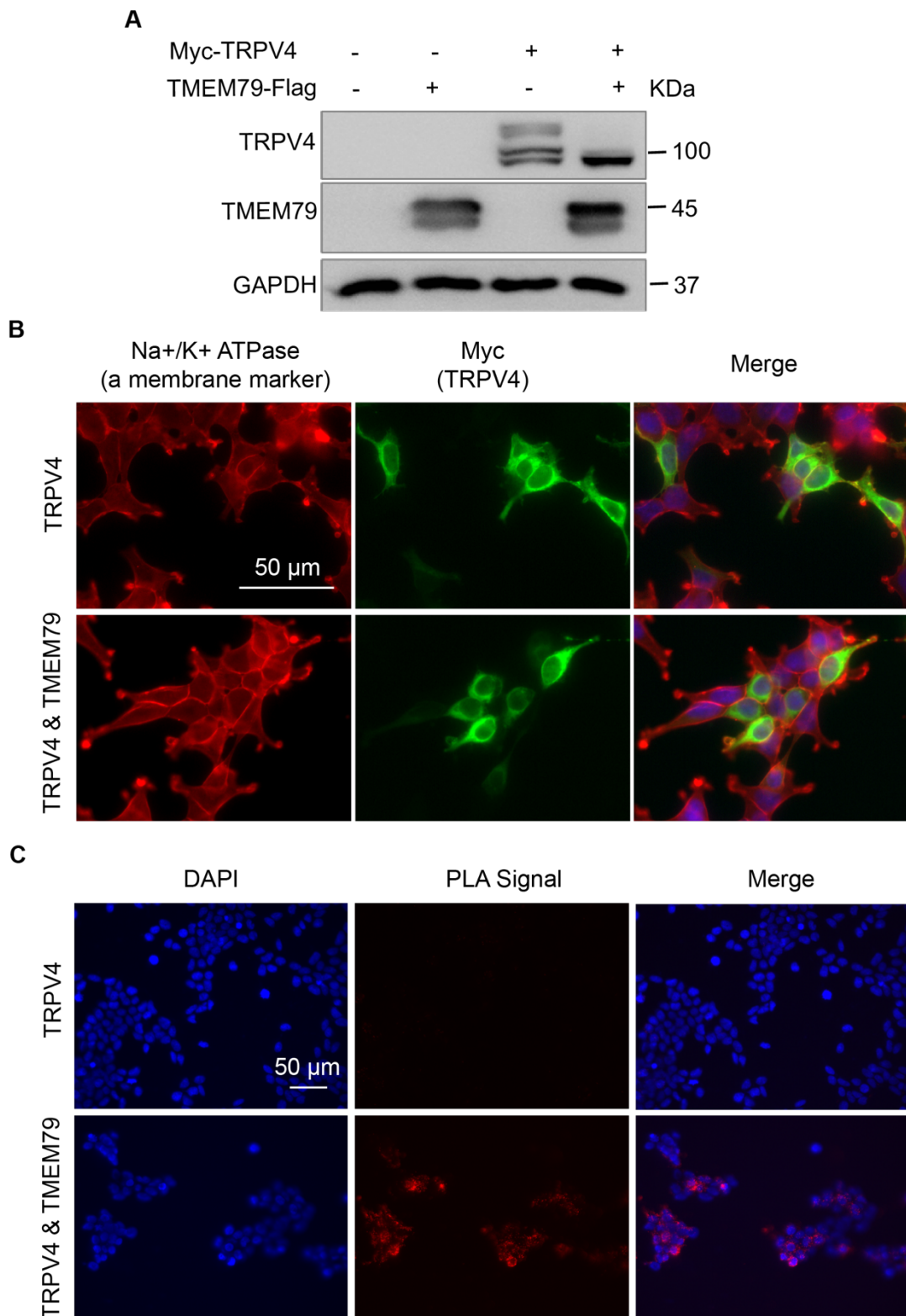


Figure 7

Potential unique interaction pattern between TRPV4 and TMEM79

(A) Western blotting of TRPV4, TMEM79, and GAPDH in HEK293 cells transiently transfected with empty vectors, myc-mTRPV4 alone, mTMEM79-flag alone, or both myc-mTRPV4 and mTMEM79-flag. When TRPV4 was expressed alone, there were three bands with sizes of approximately 96, 100, and 110 kDa, while a single band (approximately 96 kDa) was observed after co-expression with TMEM79. (B) Immunofluorescence images of TRPV4 localization. HEK293 cells transiently transfected with myc-mTRPV4 alone, or both myc-mTRPV4 and mTMEM79-flag were stained with antibodies against Na⁺/K⁺ ATPase (red) and the myc-tag (green). Nuclei were stained with DAPI (blue). Myc-mTRPV4 with or without TMEM79 showed some overlapping signal with Na⁺/K⁺ ATPase (a cell membrane marker), while it was mostly located within the cytoplasm. (C) Representative images from a PLA assay in HEK293 cells. HEK293 cells transfected with mTRPV4 alone (control) or mTRPV4/mTMEM79 were assayed using antibodies against TRPV4 and TMEM79. The PLA probes used were anti-mouse PLUS and anti-rabbit MINUS. Red puncta indicate the sites of interaction between TRPV4 and TMEM79 in HEK293 cells. Nuclei were stained with DAPI (blue). Scale bars indicate 50 μm.

Figure 8

Phenotypes and genotypes of TMEM79^{-/-} mice

(A) TMEM79^{-/-} mice exhibited an age-dependent phenotype. Compared with wild-type mice (shown on the left side in each photo), TMEM79^{-/-} mice under SPF conditions (left 3 photos) showed less fur coverage at 4 weeks old, and recovered hair phenotypes at 6 weeks old. At 10 weeks old, TMEM79^{-/-} showed matted, brown-colored fur. Under P1A conditions, TMEM79^{-/-} mice at 15 weeks old developed a chronic dermatitis phenotype. All mice were male. (B) Agarose gel electrophoresis of RT-PCR products. mRNA expression of *Trpv3*, *Trpv4*, *Tmem79*, and *β-actin* were amplified from tail keratinocytes (KCs), skin tissues of the tail, ear, back, and neck from a wild-type mouse. (C) Preparation of primary keratinocytes. Tails from male mice (3-5 weeks old) were excised, and keratinocytes were detached from the epidermal layer. The purified keratinocytes were stained with a keratinocyte marker (K14). After three days of incubation, keratinocytes were ready for the patch-clamp assay. (D) Mouse body weight. Male TMEM79^{-/-} mice (12.54 ± 0.50 , n=7) had significantly reduced body weight compared with TMEM79^{+/+} / TMEM79^{+/-} (16.17 ± 0.28 , n=9) at 3 to 5 weeks old. Statistics were performed by a two-tailed unpaired t-test. All data represent the mean \pm SEM and all error bars indicate a 95% confidence interval for the mean. *** P \leq 0.001.

Figure 9

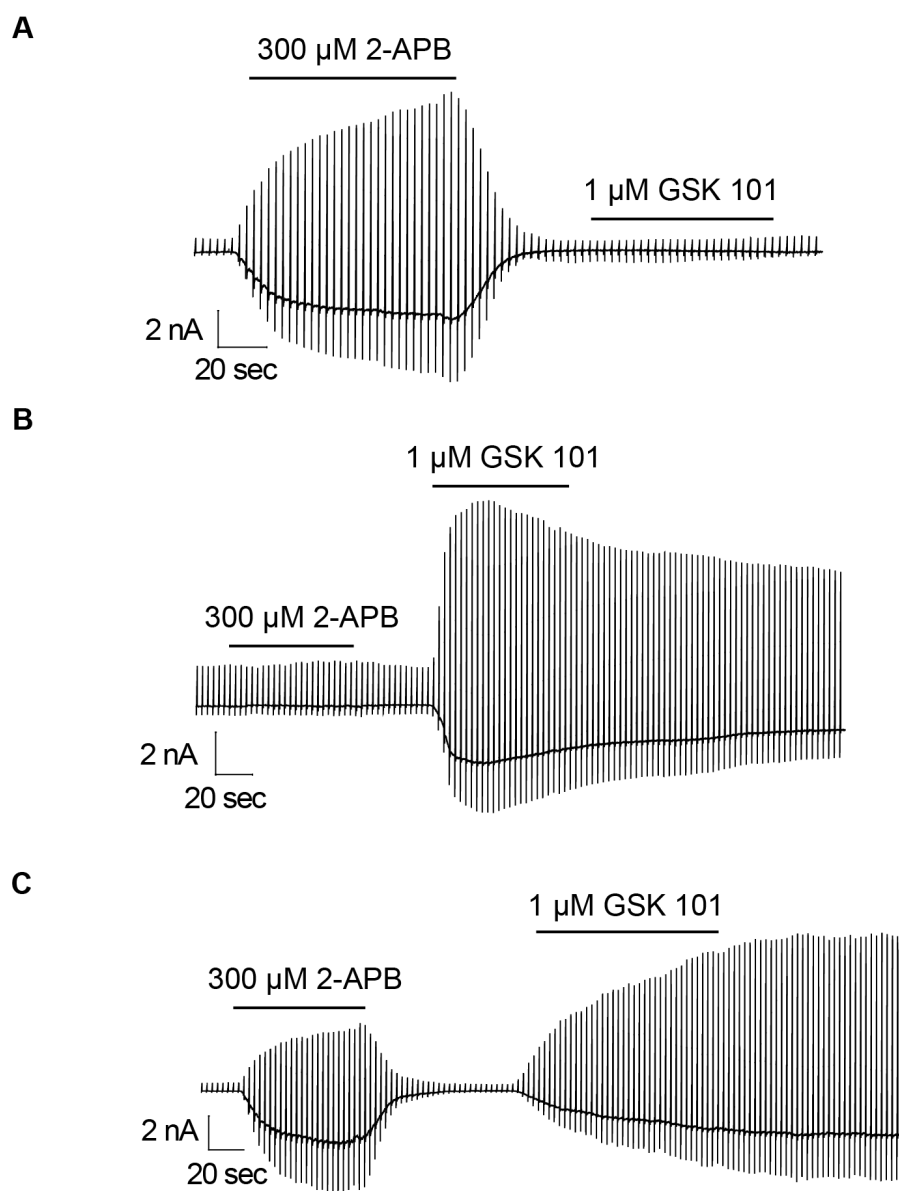


Figure 9

Most keratinocytes functionally express both TRPV3 and TRPV4.

300 μ M 2-APB and 1 μ M GSK101 induced three types of currents in WT primary keratinocytes. (A) Cells responding to 2-APB alone (12.7%). (B) Cells responding to GSK101 alone (3.2%). (C) Cells responding to both 2-APB and GSK101 (84.1%).

Figure 10

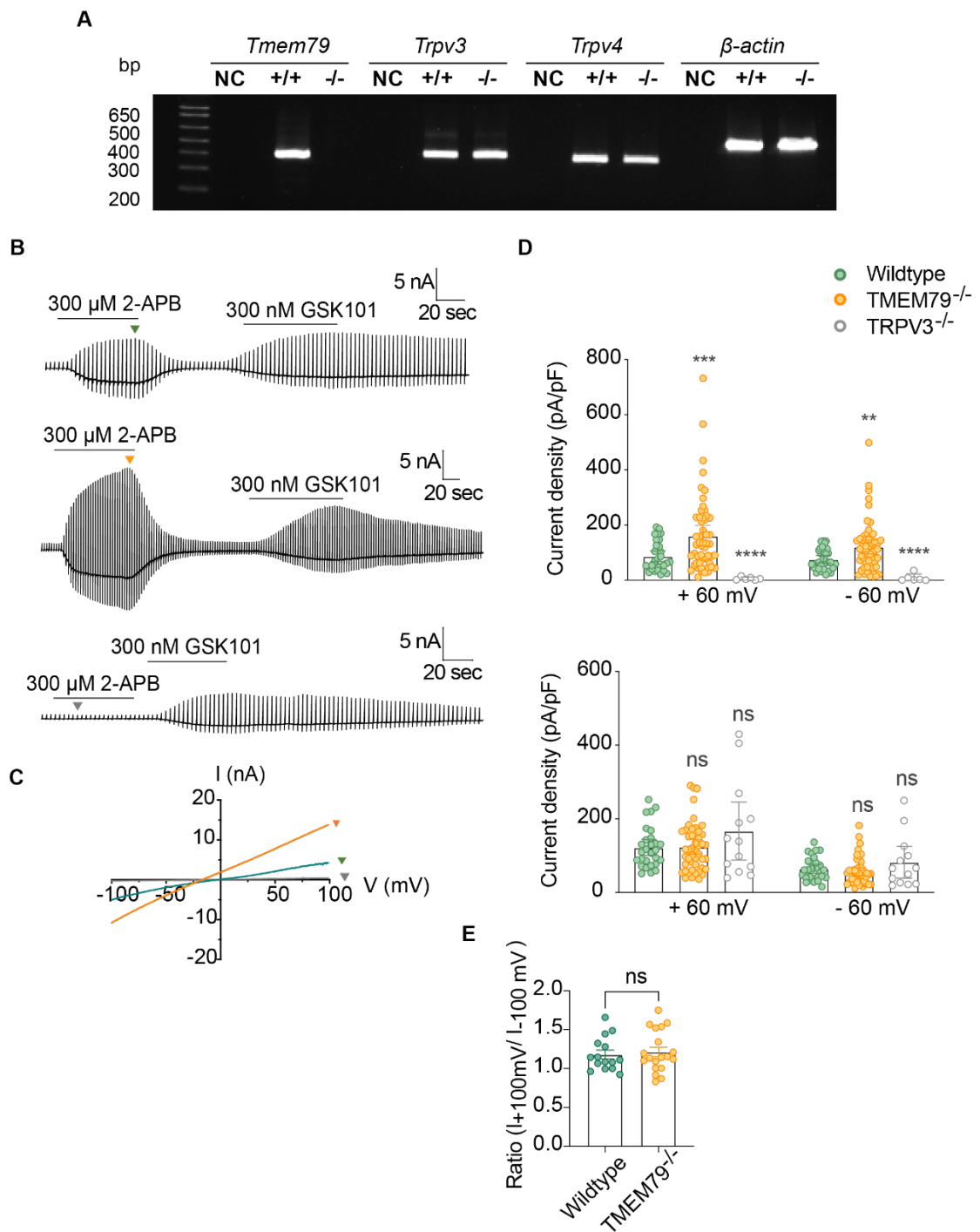


Figure 10

TMEM79 is important for TRPV3 activity in skin keratinocytes

(A) RT-PCR for *Tmem79*, *Trpv3*, *Trpv4*, and β -*actin*. Bands were amplified from tail primary keratinocytes (KCs) of wild-type and TMEM79^{-/-} mice. (B) Representative current traces evoked by 2-APB (300 μ M) and continuous GSK101 (300 nM) in keratinocytes from wild-type (top), TMEM79^{-/-} (middle), and TRPV3^{-/-} (below) mice. Recordings were performed in a ramp-pulse protocol (-100 to +100 mV) every three seconds at a holding potential of -60 mV. Scale bars indicate current amplitudes (y-axis, nA) and time (x-axis, sec). (C) I-V curves from the pulses (B) are shown in grey, green, and orange. (D) Top panel: comparison of 300 μ M 2-APB-induced current densities in primary keratinocytes from wild-type (green circles, 86.8 ± 9.5 pA/pF at + 60 mV and 75.5 ± 6.8 pA/pF at - 60 mV, n=31), TMEM79^{-/-} (orange circles, 160.7 ± 18.6 pA/pF at + 60 mV and 120.3 ± 12.4 pA/pF at - 60 mV, n=55), and TRPV3^{-/-} (grey circles, 5.9 ± 2.3 pA/pF at + 60 mV and 8.4 ± 5.6 pA/pF at - 60 mV, n=6) mice. Bottom panel: comparison of 300 nM GSK101-induced current densities in primary keratinocytes from wild-type (green circles, 122.4 ± 10.5 pA/pF at + 60 mV and 64.1 ± 6.0 pA/pF at - 60 mV, n=28), TMEM79^{-/-} (orange circles, 123.7 ± 9.6 pA/pF at + 60 mV and 56.7 ± 5.4 pA/pF at - 60 mV, n=47), and TRPV3^{-/-} (grey circles, 166.8 ± 36.2 pA/pF at + 60 mV and 82.1 ± 19.7 pA/pF at - 60 mV, n=13) mice. (E) Comparison of current ratios ($I_{+100\text{ mV}}/I_{-100\text{ mV}}$) in response to 300 μ M 2-APB between wild-type (green circles, 1.18 ± 0.06 , n=15) and TMEM79^{-/-} (orange circles, 1.22 ± 0.06 , n=19). Statistics were performed by a two-tailed unpaired t-test. All data represent the mean \pm SEM and all error bars indicate a 95% confidence interval for the mean. ** $P \leq 0.01$, *** $P \leq 0.001$, **** $P \leq 0.0001$, ns, $P > 0.05$.

Figure 11

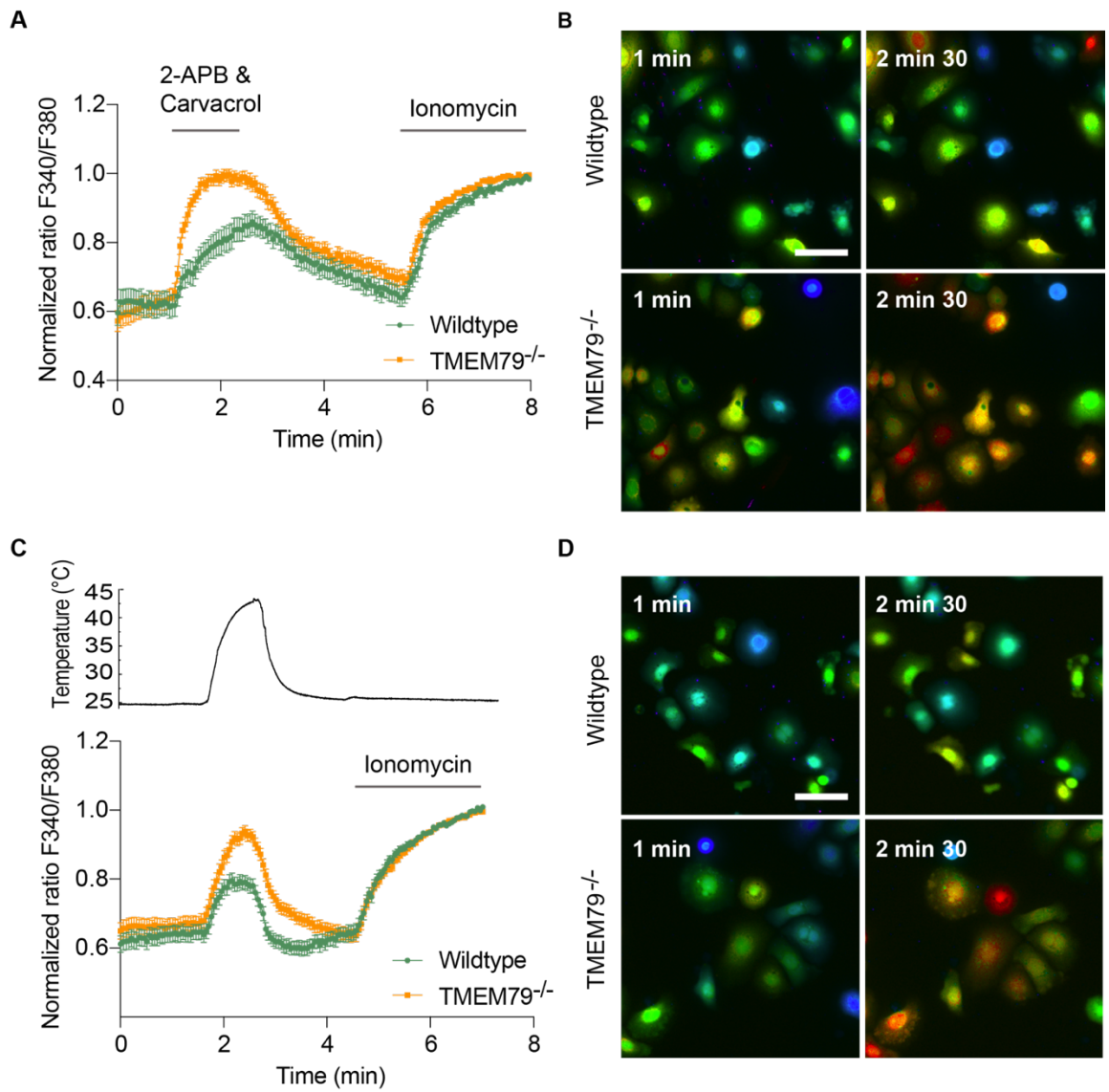


Figure 11

TRPV3 agonists and heat induce greater Ca²⁺ responses in primary keratinocytes derived from TMEM79^{-/-} mice than those from wild-type mice

(A and C) Fura-2 ratio (340/380) induced by a TRPV3 agonist cocktail (300 μ M 2-APB with 300 μ M carvacrol) (A) or heat (C) in primary keratinocytes derived from wild-type (green) and TMEM79^{-/-} (orange) mice. Recordings were performed in a 2 mM calcium standard buffer. Fura-2 ratios were normalized to 5 μ M ionomycin; n=181-303. All error bars indicate a 95% confidence interval for the mean. (B and D) Representative fluorescence images showing changes in the Fura-2 ratio in primary keratinocytes from wild-type and TMEM79^{-/-} mice in response to 300 μ M 2-APB/carvacrol (B) or heat (D). Cell images were captured at 1 min and 2 min 30 seconds. Scale bars indicate 50 μ m.

Figure 12

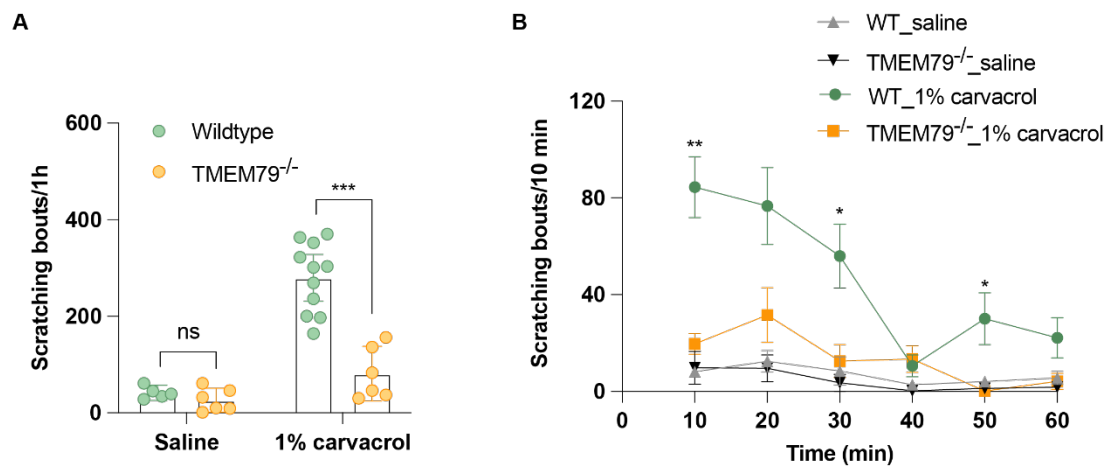


Figure 12

Carvacrol induces less scratching behavior in TMEM79^{-/-} mice than in wild-type mice

(A) Quantification of scratching bouts induced by 50 μ l saline or 1% carvacrol in wild-type (green) and TMEM79^{-/-} mice (orange). Saline induced 41.4 ± 5.6 scratching bouts in wild-type mice (n=5) and 26.5 ± 9.7 in TMEM79^{-/-} mice (n=6). Carvacrol induced 279.7 ± 21.7 scratching bouts in wild-type mice (n=11) and 81.3 ± 21.9 in TMEM79^{-/-} mice (n=6). (B) Time course of scratching behaviors in wild-type and TMEM79^{-/-} mice. All recordings were performed for 1 hour after acclimating mice for 30 min. The intradermal injection was administered to the neck of mice on the right side and the scratching bouts at the injection sites were counted. Spontaneous scratching behaviors in TMEM79^{-/-} mice were not included. Statistics were performed by a two-tailed unpaired t-test. All data and error bars in (B) represent the mean \pm SEM. Error bars in (A) indicate a 95% confidence interval for the mean. * $P \leq 0.05$, ** $P \leq 0.01$, *** $P \leq 0.001$, ns, $P > 0.05$.

Figure 13

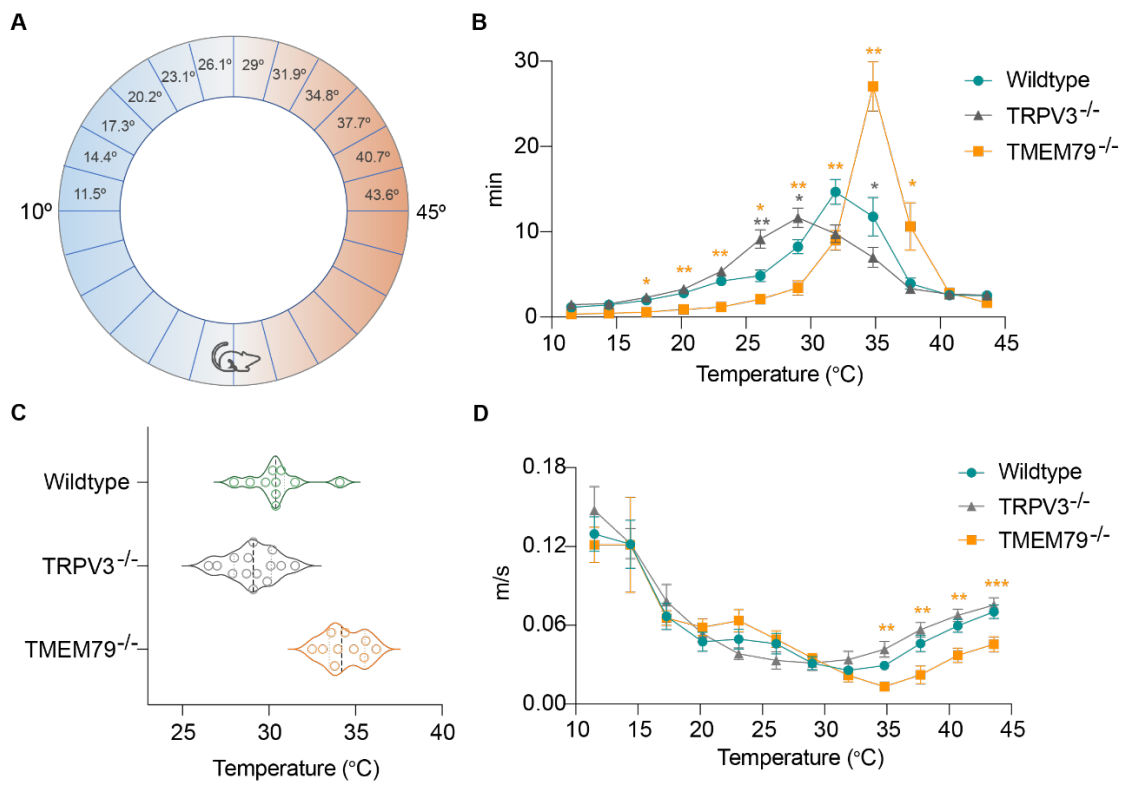


Figure 13

Thermal behavioral assay for wild-type, TRPV3^{-/-}, and TMEM79^{-/-} mice

(A) A thermal gradient ring was divided into two identical 12-zone halves ranging from 10°C to 45°C. The temperature in each zone was 11.5°C, 14.4°C, 17.3°C, 20.2°C, 23.1°C, 26.1°C, 29°C, 31.9°C, 34.8°C, 37.7°C, 40.7°C, or 43.6°C from low to high. Wild-type (green, n=10), TRPV3^{-/-} (grey, n=14), TMEM79^{-/-} (orange, n=10) mice (male, 7-10 weeks old) were released at the middle position of the thermal gradient then were allowed to freely move for 1 hour. (B) “Spent time” of wild-type, TRPV3^{-/-}, or TMEM79^{-/-} mice in each temperature zone during a 1-hour recording. (C) Violin plot of preferred temperatures for wild-type (30.4 ± 0.5), TRPV3^{-/-} (29.1 ± 0.4), or TMEM79^{-/-} (34.4 ± 0.4) mice. Mean values (grey dotted line) were calculated based on spent time. (D) Statistics were performed by a mixed-effects ANOVA with Geisser-Greenhouse correction. All data and error bars represent the mean \pm SEM. * $P \leq 0.05$, ** $P \leq 0.01$, *** $P \leq 0.001$.

Figure 14

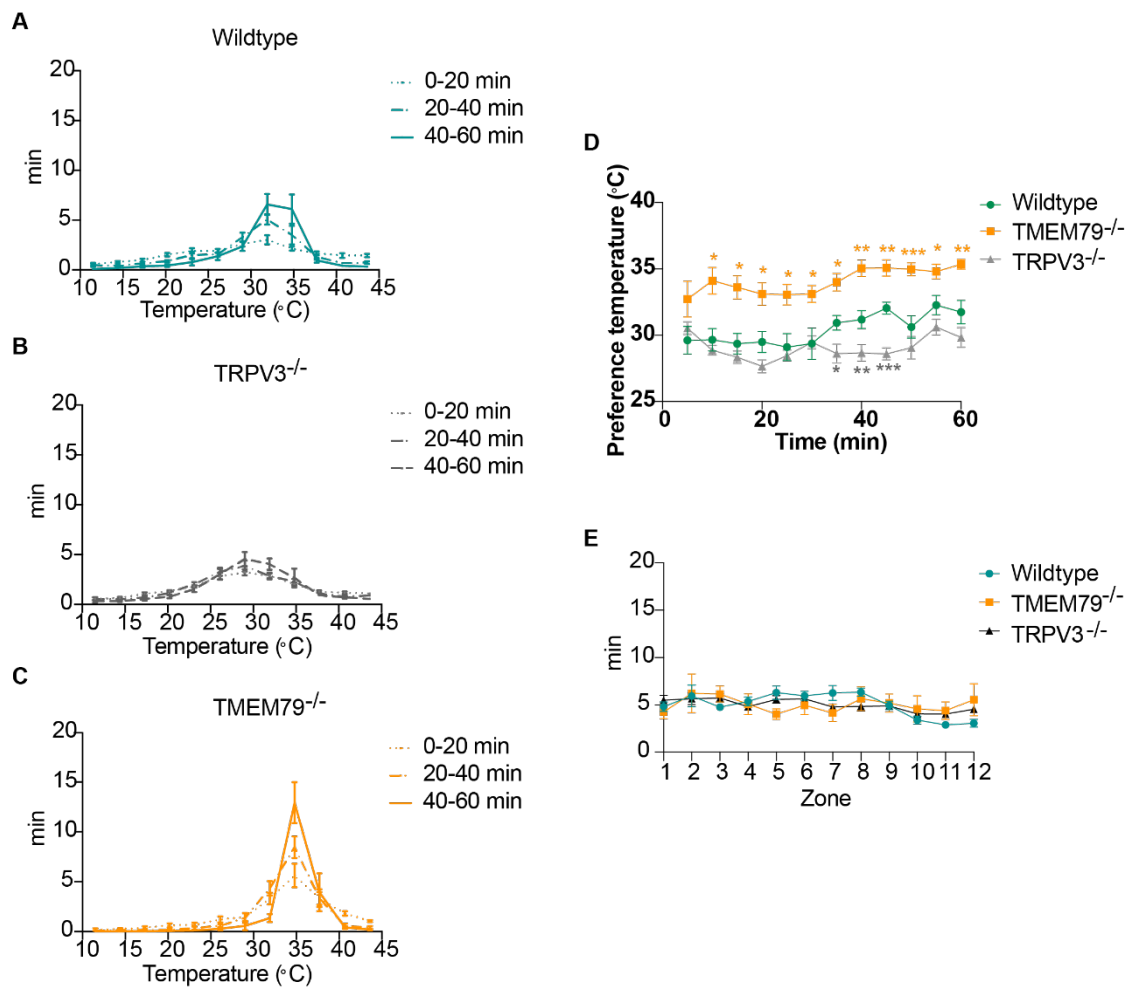


Figure 14

Thermal preference assay

(A, B, and C) “Spent time” of mice from wild-type (A), TRPV3^{-/-} (B), and TMEM79^{-/-} (C) genotypes on a thermal gradient ring with a 20-minute interval. (D) Average preferred temperature of mice at each 5-minute interval. (E) Spent time of mice on a thermal gradient ring without a thermal gradient at room temperature (25°C) during 1 hour of free movement. Data are displayed for each temperature zone, and no differences were observed among the three mouse genotypes. For each figure, n=10, 14, and 10 for wild-type, TRPV3^{-/-}, and TMEM79^{-/-} mice, respectively. All error bars represent the mean ± SEM. * P≤0.05, ** P≤0.01, *** P≤0.001.

Figure 15

A schematic working model of the interaction between TRPV3 and TMEM79

In this study, I revealed a novel interaction between TRPV3 and TMEM79. In HEK293 cells, TRPV3 and TMEM79 form a complex through which TMEM79 decreases TRPV3-mediated currents, but not TRPV4, by reducing TRPV3 expression levels in the plasma membrane. With co-expression of TMEM79, reduced TRPV3 protein expression at both the whole-cell and plasma membrane levels was achieved by reduced trafficking to the plasma membrane (#1) and increased lysosomal degradation (#2). Similarly, 2-APB-induced TRPV3-like currents were significantly larger in primary skin keratinocytes of TMEM79 knockout mice. Moreover, TMEM79 knockout mice exhibited increased occupancy in warm temperature zones in a thermal gradient assay compared with wild-type and TRPV3 knockout mice, suggesting a potential physiological role for the interaction between the two proteins *in vivo*. This figure was created with BioRender.com.

Tables

Materials and methods

Table 1 **Reagent list**

Reagent	Source	Identifier
2-Aminoethyl diphenylborinate (2-APB)	Sigma	D9754
GSK1016790A (GSK101)	Sigma	G0798
Carvacrol	Wako	030-08521
D-MEM (High Glucose) with L-Glutamine and Phenol Red	Wako	044-29765
Fetal bovine serum (FBS)	Gibco	1210446
GlutaMAX™ Supplement	Gibco	35050061
Opti-MEM™ I Reduced Serum Medium	Gibco	31985070
Protease Inhibitor	Roche	1187358000 1
Phosphatase Inhibitor (PhosSTOP)	Roche	4906845001
Lipofectamine™ Transfection Reagent	Invitrogen	18324020
PLUS™ Reagent	Invitrogen	11514015
RIPA Buffer	Thermo Scientific	89900
Protein G Mag Sepharose	Cytiva	28951379
4x Laemmli Sample Buffer	Bio-Rad	1610747
Block Ace Powder	KAC Co., Ltd	UKB80
DISPASEII	Wako	383-02281
MCDB 153 medium	CSR	CK015
Insulin	Sigma	I1882
Hydrocortisone	Sigma	H0888
O-Phosphorylethanolamine	Sigma	P0503

Transferrin	SCIPAC	P158-5
Epidermal Growth Factor	Sigma	E4127
Gentamicin	Gibco	15710064
Penicillin-Streptomycin	Gibco	15140122
Bovine pituitary extracts	Kyokuto	20200
0.25% Trypsin	Gibco	15050065
EZ-Link™ Sulfo-NHS-Biotin	Thermo	21217
Dynabeads™ MyOne™ Streptavidin T1	Invitrogen	65601
rTaq™ (Recombinant Taq DNA Polymerase)	Takana	R001
Goat serum	Sigma	G9023
ECL kit	Cytiva	RPN2232
Fura-2, AM, cell permeant	Invitrogen™	F1201
Ionomycin calcium salt from Streptomyces conglobatus	Sigma	I0634
DAPI	Dojindo	FK044
Paraformaldehyde	Wako	160-16065
Duolink® In Situ PLA® Probe Anti-Mouse PLUS	Sigma	DUO92001
Duolink® In Situ PLA® Probe Anti-Rabbit INUS	Sigma	DUO92005
Duolink® In Situ Detection Reagents Red	Sigma	DUO92008
Duolink® In Situ Mounting Medium with DAPI	Sigma	DUO82040
Sepasol-RNA I Super G	Nacalai Tesque	09379
DEPC Treated water	Invitrogen	46-2224
ReverTra Ace® qPCR RT Master Mix	Toyobo	FSQ-201
KOD FX	Toyobo	F0935K

Table 2 Antibody list

Antibody	Source	Identifier
Mouse Anti-Myc-tag (Monoclonal Antibody)	MBL	M047-3
Mouse Anti-Myc-tag (Polyclonal Antibody)	Santa Cruz	sc-789
Mouse Anti-FLAG® M2 (Monoclonal Antibody)	Sigma	F3165
Rabbit Anti-FLAG (Polyclonal Antibody)	Santa Cruz	sc-807
GAPDH-HRP conjugate (Monoclonal Antibody)	Cell Signaling	#3683
Horse Anti-mouse IgG	Cell Signaling	#7076
Goat Anti-rabbit IgG	Cell Signaling	#7074
Rabbit Anti-sodium potassium ATPase (Monoclonal antibody)	Abcam	ab76020
Mouse Anti-LAMP1 (Monoclonal Antibody)	Santa Cruz	sc-20011
Mouse Anti-Calnexin (Monoclonal Antibody)	Santa Cruz	sc-46669
Mouse Anti-TGN38 (Monoclonal Antibody)	Invitrogen	#MA3-063
Goat Anti-mouse IgG (Alexa Fluor™ 488)	Invitrogen	A-11029
Goat Anti-mouse IgG (Alexa Fluor™ 594)	Invitrogen	A-11032
Goat Anti-rabbit IgG (Alexa Fluor™ 488)	Invitrogen	A-11034
Goat Anti-rabbit IgG (Alexa Fluor™ 594)	Invitrogen	A-11037
Mouse Anti-TRPV3 (Monoclonal Antibody)	Abcam	ab85022
Rabbit Anti-TMEM79 (Polyclonal Antibody)	Novus	NBP1-59832
Mouse Anti-TRPV4		4D1 clone

Table 3 **Key equipment list**

Equipment	Source	Identifier
Luminescent image analyzer	Fujifilm	LAS-3000mini
Micropipette puller	Sutter	P-97
Manipulator controller	Sutter	MPC-200
Micromanipulator	Sutter	ROE200
Digitizer	Axon	1440A
Digital storage oscilloscope	Hitachi	VC-6723
Amplifier	Axon	200B
Thermal gradient ring	Ugo Basile	35550
Webcam	Logitech	C920
Confocal microscope	Olympus	FV3000
Conventional fluorescence microscope	Keyence	BZ-9000
Spectrophotometer	DeNovix	DS11+

Table 4 Software list

Purpose	Software
Patch-clamp recording	pCLAMP
Patch-clamp data analysis	Clampfit
Ca ²⁺ imaging and analysis	Nikon NIS-Elements AR
Thermal behavioral assay	ANY-maze software
Image analysis	ImageJ/Fiji
Data analysis and plot	Graphpad
Data analysis and plot	Origin
Data integration	Microsoft Excel
Figure preparation	Adobe Illustrator

Table 5

Primer list for genotyping (# 1-3), RT-PCR (# 4-11), and qPCR (# 12-15).

Primer order (#)	Primer name	Sequence (5'-3')
1	<i>Tmem79-Intron1-F</i>	ATCCTCCATTTTCGCTCCTCTGC
2	<i>Lar3-universal-R</i>	CACAACGGGTTCTTCTGTTAGTCC
3	<i>Tmem79-Exon2-R</i>	CTAGGGGCTCTGGTTCAATATC
4	<i>Trpv3-Exon15-F</i>	GGACTGCAGTTCCTATGGCA
5	<i>Trpv3-Exon17-R</i>	TGCTGTCCGTCTTATGGGTC
6	<i>Trpv4-F</i>	ACAACACCCGAGAGAACACC
7	<i>Trpv4-R</i>	CCCAAACCTTACGCCACTTGT
8	<i>Tmem79-Exon1-F</i>	CCTTTCCCATCGTACTCGGG
9	<i>Tmem79-Exon3-R</i>	CGAGCATGGTCAGGGTAGTC
10	<i>β-actin-F</i>	TGTTACCAACTGGGACGACA
11	<i>β-actin-R</i>	AAGGAAGGCTGGAAAAGAGC
12	<i>Trpv3-Exon2-F</i>	ACGGTCACCAAGACCTCTC
13	<i>Trpv3-Exon3-R</i>	GACTGTTGGGATTGGATGGGG
14	<i>Gapdh-F</i>	CATCACTGCCACCCAGAAGACTG
15	<i>Gapdh-R</i>	ATGCCAGTGAGCTTCCCGTTCAG

Acknowledgments

Here, I would like to offer my sincere appreciation to my PhD supervisor Dr. Makoto Tominaga for his kind and patient support in my research and daily life. Over the past three years, I have obtained certain knowledge and skills in the physiology field and have become more independent under his supervision. I would like to thank Dr. Masayuki Amagai and Dr. Takeshi Matsui (Keio University) for providing the TMEM79 knockout mice. I would like to thank Dr. Takaaki Sokabe, Dr. Shigeru Saito, and Dr. Takuto Suito for their encouraging suggestions to improve my thesis. I would like to thank Naomi Fukuta, Claire Saito, Keiko Fukuoka, and Terumi Hashimoto for their assistance in acquiring the experimental materials and animal care. I would like to thank Yoshimi Ito for handling a lot of paperwork, which helped me to overcome language difficulties. I would like to thank my advisors Dr. Tomomi Nemoto and Dr. Hideji Murakoshi for their kind suggestions helping my progress. I would like to thank Dr. Tianbang Li for helping me get started with patch-clamp experiment, which was the first technique I learned after entering this lab. I would like to thank Dr. Yu Yamanoi for teaching me keratinocyte isolation. I would like to thank Dr. Tatsuhiko Kadowaki for the enlightenment provided towards my research. Without his encouragement, I would not have challenged myself. I would like to also thank the other lab members, Dr. Makiko Kashio, Dr. Kenta Maruyama, Dr. Shoma Sato, Dr. Derouiche Sandra, Dr. Xiaona Feng, Dr. Nguyen Thi Hong Dung, Aykut Deveci, Xingmei Deng, and Aliyu Mudassir Magaji, for their support and companionship during my PhD life. Finally, I am deeply grateful to all of my family for their unreserved support. Although I was not able to visit them during the pandemic, I always felt encouraged by our weekly video chats.